Magnetic Resonance Imaging Data Phenotypes for the Parkinson's Progression Markers Initiative

Brian B Avants[1,2], Leon Fonville[1], Olivia Hampton[1], Alexandra Reardon[1], Andrew Stenger[1], Xue Wang[1], Nicholas J Tustison[2], James R Stone[2], Philip A Cook[3], Barbara Marebwa[4], Lana M Chahine[5], Kathleen L Poston[6], Kenneth Marek[7], Lino Becerra[1], Roger Gunn[1] for the Alzheimer's Disease Neuroimaging Initiative*

[1]Invicro, Needham, MA, USA

[2]Department of Radiology and Medical Imaging, University of Virginia, Charlottesville, VA, USA

[3]Department of Radiology, University of Pennsylvania, Philadelphia, PA

[4]Parkinson's Research, The Michael J. Fox Foundation, New York City, New York, USA

[5]Department of Neurology, University of Pittsburgh, Pittsburgh, PA, USA

[6]Department of Neurology, Stanford University, Palo Alto, CA, USA

[7]Institute for Neurodegenerative Disorders, New Haven, CT, USA

Corresponding author:
Brian B. Avants
avants@grasp.cis.upenn.edu

*Data used in preparation of this article were obtained from the Alzheimer's Disease Neuroimaging Initiative (ADNI) database (adni.loni.usc.edu). As such, the investigators within the ADNI contributed to the design and implementation of ADNI and/or provided data but did not participate in analysis or writing of this report. A complete listing of ADNI investigators can be found at: http://adni.loni.usc.edu/wp-content/uploads/how_to_apply/ADNI_Acknowledgement_List.pdf

Abstract

The Parkinson's Progression Markers Initiative (PPMI) delivers multiple modality MRI (M3RI) and biomarker data for a comprehensive longitudinal study of Parkinson's Disease (PD). These provide quantitative indices of deep brain and cortical structure (T1-weighted MRI), microstructural integrity of brain tissue (diffusion-weighted imaging) and resting brain function (resting state functional MRI). Integrating and uniformly analyzing M3RI alongside non-imaging biological and clinical data is challenging due to the distinct nature of each modality. This study systematically organizes these complex data into a structured format, provides a PD-focused evaluation of the methodologies and evidence for technical robustness of the approach. The cohort encompasses 841 idiopathic PD, 309 genetic PD, 1364 presymptomatic PD and 240 control subjects at baseline with followup at a mean of 1.83 years.

Background & Summary

Parkinson's Disease (PD) is characterized by the progressive accumulation of Lewy bodies, primarily composed of misfolded alpha-synuclein, and appearing in the substantia nigra at an early stage (Fearnley and Lees 1991). The spread of this pathology correlates with both motor and non-motor symptoms of PD, underscoring alpha-synuclein's pivotal role in disease progression (Lee and Trojanowski 2006; Dickson et al. 2009; Calabresi et al. 2023). The synuclein amplification assay (SAA) significantly advanced PD research by enabling in vivo confirmation for the first time. The Parkinson's Progression Markers Initiative (PPMI) study enhances this development by offering a comprehensive dataset of subjects assessed with SAA and multimodal MRI (M3RI), facilitating the monitoring of PD progression and the impact of synucleinopathy on brain structure and function (Shahnawaz et al. 2020; Siderowf et al. 2023).

Analyzing longitudinal M3RI in the PPMI study necessitates accessible data representations for the PD research community. While each MRI modality provides distinct insights, their combined analysis is challenging due to the data's high dimensionality and computational demands. Therefore, creating clear, accessible data representations is crucial for advancing PD research and fostering new discoveries in particular using multi-view data linking evidence of pathology, symptoms and imaging (Nemmi et al. 2019; Tremblay et al. 2020; Markello et al. 2021).

The study utilizes the Advanced Normalization Tools X (ANTsX) ecosystem to process PPMI MRI from 2010 to early 2024, focusing on T1-weighted, diffusion-weighted, and resting-state functional rsfMRI. The extended duration of data collection underscores the necessity for robust processing techniques that manage the resultant heterogeneity in images. ANTsX, leveraging decades of MRI analysis expertise, employs advanced techniques and integrates open science, deep learning, and machine learning for efficient multi-site M3RI data processing

(B. B. Avants et al. 2015; Stone et al. 2020; Tustison et al. 2021)

To establish face validity, this study leverages not only PPMI M3RI, but also the Alzheimer's Disease Neuroimaging Initiative (ADNI) (Veitch et al. 2024) and traveling subject data in three cohorts (Hawco et al. 2022; Tanaka et al. 2021; Tong et al. 2019). We analyze these data collectively and uniformly to establish reliability benchmarks and to demonstrate feasibility of consistent processing in multi-site studies such as PPMI. Additionally, we exemplify statistical models using PPMI data that are appropriate for unlocking key questions relevant to biomarker-confirmed PD and related conditions.

Historically, MRI research on PD has primarily utilized T1-weighted (T1w) structural imaging to investigate neuroanatomical changes. A consistent finding across these studies has been the identification of early neurodegeneration in mid-brain regions, particularly the substantia nigra (Schwarz et al. 2011; Aquino et al. 2014; Ryman and Poston 2020; Poston et al. 2020). Diffusion-weighted MRI (dwMRI) has further enhanced our understanding by allowing for the investigation of white matter microstructural integrity which may be impacted not only in sporadic PD (Péran et al. 2010; Owens-Walton et al. 2024) but also in genetic PD (Tolosa et al. 2020; Owens-Walton et al. 2024). Similarly, resting state functional MRI (rsfMRI) has unveiled alterations in network connectivity in PD patients, highlighting changes in the functional integration and segregation of brain networks involved in motor and cognitive functions (Hacker et al. 2012; Kim et al. 2017; Esposito et al. 2013). Taken together, these findings suggest that PD impacts both the structural and functional aspects of the brain. More integrative research in PD (Menke et al. 2009; Markello et al. 2021) is needed to determine the sequence of these changes and how they may relate to alpha-synuclein and potential copathology or comorbidity (Simuni et al. 2024).

The present study extends previous foundations by providing standardized imaging data phenotypes (IDPs) for PPMI with a particular emphasis on an accessible tabular representation. The summary IDPs are computed with ANTsPyMM v1.4.0 and depend on standard anatomical and functional hierarchies that are well-established in the field and consistently integrated in this work across modalities. This approach supports investigations based on T1w structural imaging, dwMRI, and rsfMRI either independently or collectively. Importantly, these imaging variables easily merge with the associated demographics, SAA status, clinical data such as the Movement Disorder Society-Sponsored Unified Parkinson's Disease Rating Scale (MDS-UPDRS) (Disease 2003) and standard PPMI DAT-SPECT summary measurements (Bega et al. 2021; Droby et al. 2022). Through this integrative methodology, we aim to contribute to a deeper understanding of PD, facilitating the development of more effective diagnostic and therapeutic strategies and accelerating PD research.

Methods

MRI data collection

MRI data collection occurred between 2010 and an April 2024 cutoff date for these data. Two phases of MRI collection occurred in PPMI; the first collected T1w and later DTI as part of exploratory investigations. In 2020, a new phase of collection sought to improve both MRI quality and consistency and expand the number of modalities collected. The sequences used at each site are provided in detail at (B. Avants 2024) and in the original Laboratory of Neuroimaging (LONI) source data (described below in Data Records). The "phase" of data collection is captured in the variable `imaging_protocol`. The PPMI data includes control subjects, idiopathic (sporadic) PD subjects and genetic PD subjects characterized by GBA, LRRK2, SNCA and PRKN mutations; the latter two groups appear infrequently in this PPMI M3RI cohort. Additionally, presymptomatic subjects comprise a substantial and growing portion of the cohort; these are also characterized by genetic mutations and/or early risk factors for PD (hyposmia or RBD) (Siderowf et al. 2023). Table 1 summarizes the cohort characteristics. In the following sections, we focus on the PD cohort with SAA measurements as the presymptomatic cohort is undergoing significant additional data collection.

Data Organization

Raw DICOM data was downloaded from LONI and converted to nifti format via `dcm2niix` (Li et al. 2016). These data were then organized into a directory tree following the NRG format illustrated in Figure 1. This BIDS-like structure (Gorgolewski et al. 2016) is defined to aid in longitudinal analyses of multiple modality data and intends to support: (a) sortable and specific dates associated with imaging sessions; (b) links between the data on disk and its origin (LONI) through the "Image ID"; (c) easy maintenance of multiple modality data collections; and (d) predictable input/output structure. Critically, the unique ID allows the original data associated with an IDP to be easily found in LONI. In brief, this system assigns each image – and categories of derivative data – a directory and individual file name that assist in making data findable, accessible, interpretable and reproducible (FAIR) for both early and downstream processing.

ANTsPyMM processing

ANTsPyMM collects and documents best ANTsX practices for both data inspection and IDP generation for the modalities of interest in a single python package. While ANTsPyMM supports BIDS format, it behaves most predictably and safely with NRG format. Each "run" of the integrated multiple modality processing encoded by ANTsPyMM is driven by a data frame that defines a multiple modality "collection" of images for a given subject at a given date. There are two key functions that aid users in defining the appropriate input data structure and sending

Table 1. Baseline PPMI IDP cohort. AR=at-risk; MSA = multi-system atrophy; OtherGen = other genetic; RBD = REM Sleep Behavior Disorder.

	CN (N=748)	**GenAR (N=553)**	**SporadicAR (N=811)**	**OtherGenPD (N=10)**	**LRRK2PD (N=185)**	**GBAPD (N=119)**	**SporadicPD (N=851)**	p
age	69.8 ± 9.8	62.3 ± 7.4	68.1 ± 5.6	49.9 ± 14.0	64.9 ± 8.5	62.2 ± 9.6	63.6 ± 9.2	< 0.001
Sex								< 0.001
Female	356 (47.6%)	331 (59.9%)	400 (49.3%)	2 (20.0%)	98 (53.0%)	54 (45.4%)	308 (36.2%)	
Male	392 (52.4%)	222 (40.1%)	411 (50.7%)	8 (80.0%)	87 (47.0%)	65 (54.6%)	543 (63.8%)	
race								< 0.001
Asian	4 (0.5%)	0 (0.0%)	3 (0.4%)	0 (0.0%)	1 (0.5%)	0 (0.0%)	14 (1.6%)	
Black	10 (1.3%)	0 (0.0%)	6 (0.7%)	0 (0.0%)	0 (0.0%)	2 (1.7%)	11 (1.3%)	
not.spec.	507 (67.8%)	6 (1.1%)	8 (1.0%)	0 (0.0%)	0 (0.0%)	0 (0.0%)	6 (0.7%)	
Other	8 (1.1%)	12 (2.2%)	27 (3.3%)	0 (0.0%)	14 (7.6%)	2 (1.7%)	24 (2.8%)	
White	219 (29.3%)	535 (96.7%)	767 (94.6%)	10 (100.0%)	170 (91.9%)	115 (96.6%)	796 (93.5%)	
duration.yrs		0.8 ± 1.2		3.6 ± 3.7	3.0 ± 2.1	2.7 ± 1.9	0.7 ± 0.6	< 0.001
updrs.totscore	4.8 ± 4.4	9.5 ± 8.8	13.1 ± 10.4	33.1 ± 16.7	37.4 ± 17.7	45.5 ± 14.9	35.0 ± 15.1	< 0.001
CSFSAA								< 0.001
Negative	474 (86.2%)	484 (92.4%)	127 (35.8%)	4 (50.0%)	61 (35.7%)	6 (6.7%)	49 (7.4%)	
Positive	76 (13.8%)	39 (7.4%)	226 (63.7%)	4 (50.0%)	109 (63.7%)	82 (91.1%)	608 (92.3%)	
PosMSA	0 (0.0%)	1 (0.2%)	2 (0.6%)	0 (0.0%)	1 (0.6%)	2 (2.2%)	2 (0.3%)	
LEDD	0.0 ± 0.0	4.1 ± 45.8	0.4 ± 10.5	573.2 ± 450.4	465.0 ± 425.7	542.3 ± 551.3	9.9 ± 62.6	< 0.001
subgroup								< 0.001
GBA	0 (0.0%)	281 (50.8%)	0 (0.0%)	0 (0.0%)	0 (0.0%)	119 (100.0%)	0 (0.0%)	
GBA + RBD	0 (0.0%)	1 (0.2%)	0 (0.0%)	0 (0.0%)	0 (0.0%)	0 (0.0%)	0 (0.0%)	
Healthy Control	242 (100.0%)	0 (0.0%)	0 (0.0%)	0 (0.0%)	0 (0.0%)	0 (0.0%)	0 (0.0%)	
Hyposmia	0 (0.0%)	0 (0.0%)	567 (69.9%)	0 (0.0%)	0 (0.0%)	0 (0.0%)	0 (0.0%)	
LRRK2	0 (0.0%)	245 (44.3%)	0 (0.0%)	0 (0.0%)	178 (96.2%)	0 (0.0%)	0 (0.0%)	
LRRK2 + GBA	0 (0.0%)	24 (4.3%)	0 (0.0%)	0 (0.0%)	7 (3.8%)	0 (0.0%)	0 (0.0%)	
PRKN	0 (0.0%)	0 (0.0%)	0 (0.0%)	5 (50.0%)	0 (0.0%)	0 (0.0%)	0 (0.0%)	
RBD	0 (0.0%)	0 (0.0%)	244 (30.1%)	0 (0.0%)	0 (0.0%)	0 (0.0%)	2 (0.2%)	
SNCA	0 (0.0%)	2 (0.4%)	0 (0.0%)	5 (50.0%)	0 (0.0%)	0 (0.0%)	0 (0.0%)	
Sporadic PD	0 (0.0%)	0 (0.0%)	0 (0.0%)	0 (0.0%)	0 (0.0%)	0 (0.0%)	849 (99.8%)	
imaging.protocol								< 0.001
ADNI	506 (67.6%)	0 (0.0%)	0 (0.0%)	0 (0.0%)	0 (0.0%)	0 (0.0%)	0 (0.0%)	
PPMI1	169 (22.6%)	538 (97.3%)	60 (7.4%)	3 (30.0%)	172 (93.0%)	110 (92.4%)	388 (45.6%)	
PPMI2	73 (9.8%)	15 (2.7%)	751 (92.6%)	7 (70.0%)	13 (7.0%)	9 (7.6%)	463 (54.4%)	

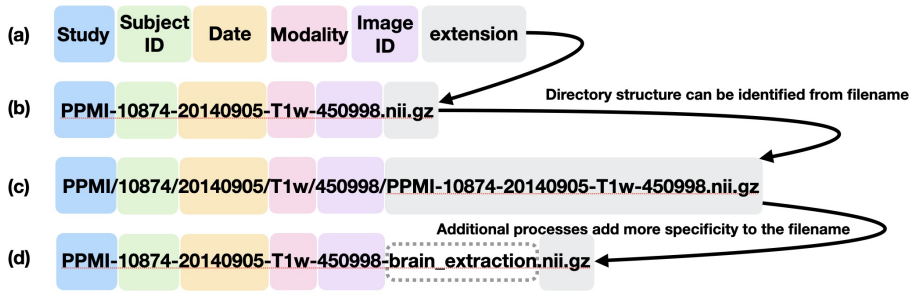

Figure 1: The NRG format supports predictable and interpretable data storage and processing that can easily be tied back to the LONI source dicom. The filename proceeds from less specific information (Project ID at reader's left) to the most specific (unique image ID at reader's right). A specific character – here the dash – is reserved exclusively as a separator between the stages of information.

that data to processing. The first is `antspymm.generate_mm_dataframe` which generates the appropriate multiple modality subject dataframe that documents on disk locations for image sets. The resulting dataframe defines the expected input as well as output structures. The second key function runs the multiple modality processing (`antspymm.mm_csv`) based on the multiple modality subject dataframe. The "Usage Notes" section provides more details on this system with an accompanying reproducible example based on freely accessible multiple modality neuroimaging.

Semi-automated quality assessment

ANTsPyMM's primary goal is reliable M3RI IDP generation. Of necessity, it also addresses quality control (QC) with particular focus on the T1w modality i.e. the core anatomical image that represents the most consistently collected MRI in PPMI. T1w is the focus of QC because ancillary modality processing depends heavily on anatomical labels (e.g. tissue segmentation, cortical parcellation) derived from these images. As such, we developed an automated (deep learning based) T1w reviewer that is trained on human (BA) QC reviews. Each T1w image is therefore reviewed internally in the first stage of ANTsPyMM processing by this `resnetGrader` (a deep learning model trained to predict image quality) (B. Avants et al. 2023). The grader will abort processing if the T1w does not achieve a given baseline level of quality. Human visual inspection was performed on images that pass the grader by BA and serves as a sanity check to the automated method. The `resnetGrader` successfully filtered unusable data and we selected a quality cutoff at 1.02 to filter out low quality images. Similarly, the rsfMRI and DTI were reviewed in `post hoc` fashion. This process involved visually inspecting each estimated FA image and each estimated default mode network connectivity map and its associated mean BOLD image. Particular

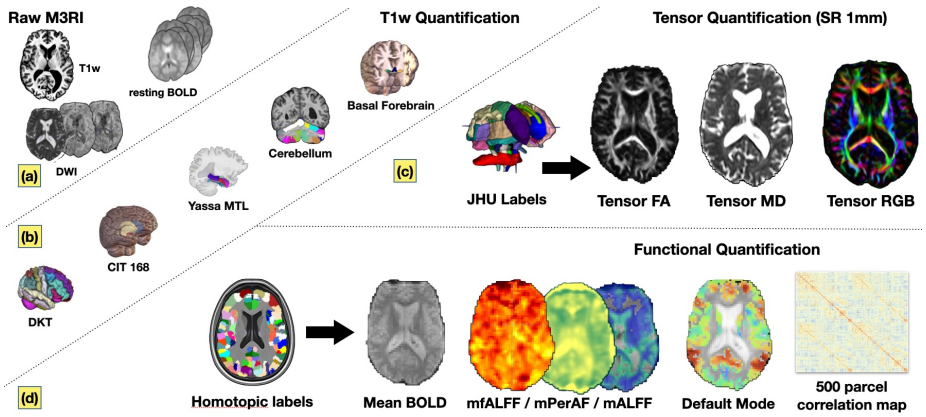

Figure 2: Overview of ANTsPyMM outputs for T1-weighted MRI, diffusion MRI and resting state fMRI. Panel (a) shows example input data; the package does not require all modalities to be present – only T1w. It also handles arterial spin labeling (perfusion), FLAIR and neuromelanin, not covered here. Panel (b) illustrates core T1w outputs across several inter-related and PD relevant systems in the brain. Panel (c) shows the standard outputs associated with DTI. Whole brain tractography is also output but no evaluation results are available to contextualize its performance and, as such, we do not recommend its use. Panel (d) summarizes the various rsfMRI outputs for processing parameter set number 129 referred to with a prefix `rsfMRI_fcnxpro129`.

focus was paid to cases with high motion and/or low SNR; such images were excluded from statistical analyses.

Neuroanatomical coordinate systems

The statistical interpretation of processed images is aided by automatic anatomic labeling with pre-specified coodinate systems or maps overlaid on each subject's neuroimage. We leverage a recent homotopic parcellation (Yan et al. 2023), the Desikan-Killiany-Tourville (DKT) system (Klein and Tourville 2012), the CIT168 atlas (Pauli, Nili, and Tyszka 2018), the Johns Hopkins University (JHU) white matter labels (Mori, Oishi, and Faria 2009), the Schmahmann cerebellar parcellation (Lyu et al. 2024; Carass et al. 2018), brain stem labels (Iglesias et al. 2015), a medial temporal lobe schema (Rizvi et al. 2023) and labels derived from probabilistic maps of the basal forebrain (Liu et al. 2015; Zaborszky et al. 2008). These systems are described in detail in online data dictionary and associated documentation for this project. These coordinate system enable PD researchers to interrogate a variety of hypotheses related to, for example, known functional networks, association hubs, cholinergic networks, the striatum or dopaminergic systems.

T1-weighted MRI processing

T1-weighted MRI processing is described in detail in (Tustison et al. 2023, 2021). This open-source software ecosystem includes tools for image registration, segmentation, and super-resolution (SR) as customized for the human brain. The derived measurements are tabulated by the neuroanatomical coordinates defined above and include cortical and subcortical measurements and morphological measurements of the hippocampus, basal forebrain and cerebellum. The results of this stage are key to consistent processing of rsfMRI and DWI. We provide both original resolution (OR) and SR results as part of this effort. For SR processing of T1w, the network is applied – first – over the whole head T1w image to double resolution along all axes within the brain parenchyma. Otherwise, SR and OR processing are identical. SR training with 3D perceptual losses is documented in the `python` package siq and is based on `tensorflow` implementations of a volumetric deep back projection network (DBPN) (B. Avants et al. 2023; Tustison et al. 2021; Haris, Shakhnarovich, and Ukita 2020) . See Figure 2 for examples of these outputs. IDPs derived from the T1 processing are denoted by prefixes `T1w` and `T1Hier`.

Diffusion weighted MRI processing

Diffusion tensor image (DTI) processing leverages best practices from both ANTsX (B. B. Avants et al. 2015; Stone et al. 2023, 2020) and the open-source DTI-focused project DiPy (Garyfallidis et al. 2014). This pipeline is specifically designed to utilize DWI acquisitions with either a single or opposed phase encoding directions. The functionality has been developed to address a broad

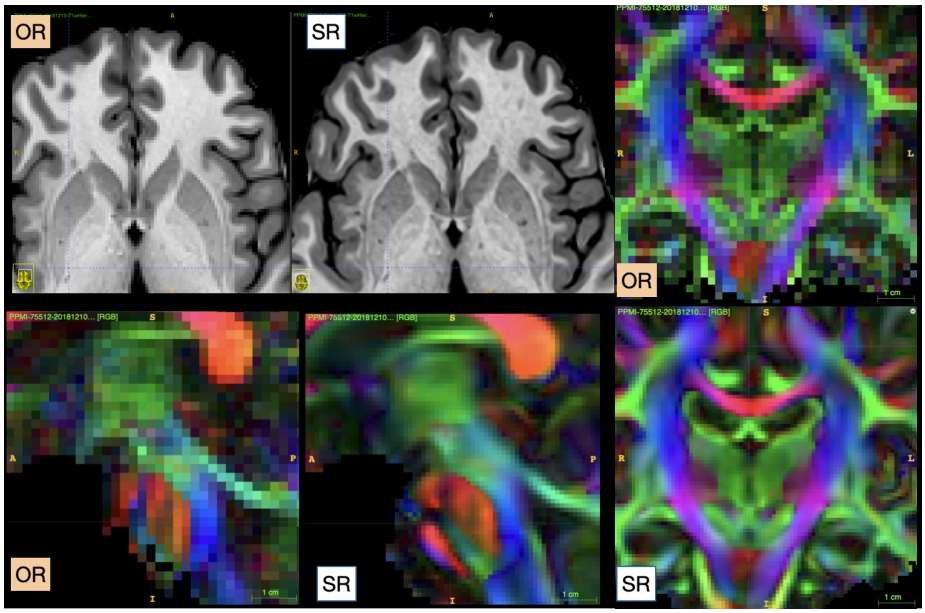

Figure 3: Example ANTsPyMM SR outputs applied to T1-weighted MRI (upper left) and diffusion MRI. T1w is super resolved to 0.5mm isotropic and DTI to 1mm.

spectrum of preprocessing requirements, such as motion correction, denoising, dewarping and gradient reorientation, and enhancement through SR techniques, culminating in an optimized DTI reconstruction. The SR stream applies to each volume in the DWI timeseries after motion correction and distortion correction but before tensor fitting i.e. in a relatively minimally invasive fashion. After reconstruction, the pipeline integrates atlas-based labeling and template-based normalization processes, thereby enhancing the anatomical interpretability of the DTI metrics. Figure 4 summarizes the pipeline which follows these steps:

1. **Input Preparation**: The pipeline accepts either a single DWI or a pair of DWI with reversed phase encoding. It also requires associated b-values and b-vectors for each direction, alongside a T1-weighted image and a brain mask for improved spatial accuracy in inter-modality registration.

2. **Initial Reconstruction and Motion Correction**: By default, the DWI data is denoised before performing motion correction. This is skipped when applying SR which integrates denoising. Motion correction aligns DWI volumes within and across acquisitions to a reference mean B0 and mean DWI, reducing artifacts due to subject movement.

3. **Dewarping and Super-Resolution**: Dewarping is applied to correct for distortions between the DWI space and the T1-weighted image. Optionally, SR is applied after dewarping but before the DiPy based reconstruction

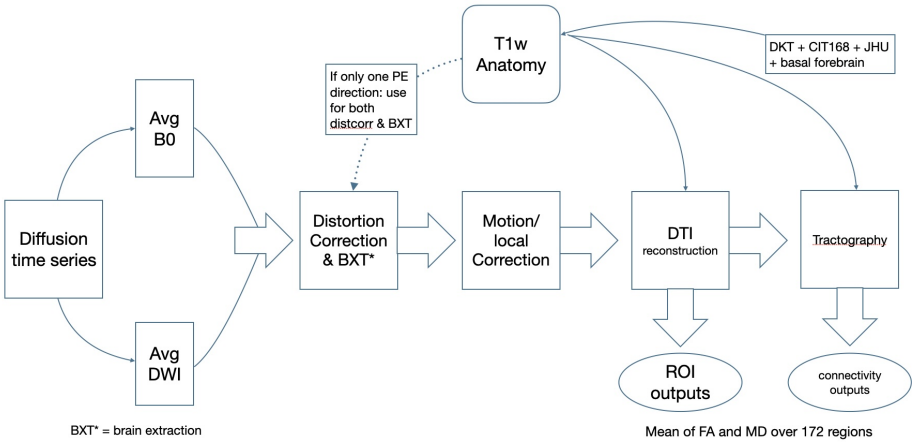

Figure 4: Overview of the DTI processing pipeline based on ANTsX and DiPy.

process.

4. **Reconstruction of DTI Metrics**: The function employs weighted least squares to reconstruct DTI metrics such as Fractional Anisotropy (FA) and Mean Diffusivity (MD) from the preprocessed DWI data. This step is pivotal in quantifying the diffusion properties of brain tissue.

5. **Atlas-Based Labeling and Registration**: Utilizing the Johns Hopkins University (JHU) atlas and corresponding labels (Mori, Oishi, and Faria 2009), the pipeline performs spatial registration of the DTI to the atlas space. This process facilitates anatomical localization and quantification of DTI metrics within predefined brain regions.

6. **Output Generation**: The pipeline yields a comprehensive output including the reconstructed DTI metrics, summary statistics of these metrics within atlas-defined regions, the spatial registration information, and additional diagnostic metrics such as framewise displacement and signal-to-noise ratio (SNR) assessments spatially and temporally for both B0 and DWI. An example output volumetric tensor image with labels is in Figure 3 and 5.

IDPs derived from the DWI processing are denoted by prefixes `DTI_`.

Resting state functional MRI processing

Resting state functional MRI (rsfMRI) processing builds on prior multi-view M3RI analyses performed in this same ecosystem (B. B. Avants et al. 2015, 2019; B. B. Avants, Tustison, and Stone 2021). The procedure is based on the findings described in three comprehensive evaluation studies (Shirer et al. 2015; Parkes et al. 2018; Noble, Scheinost, and Constable 2019) and is designed to

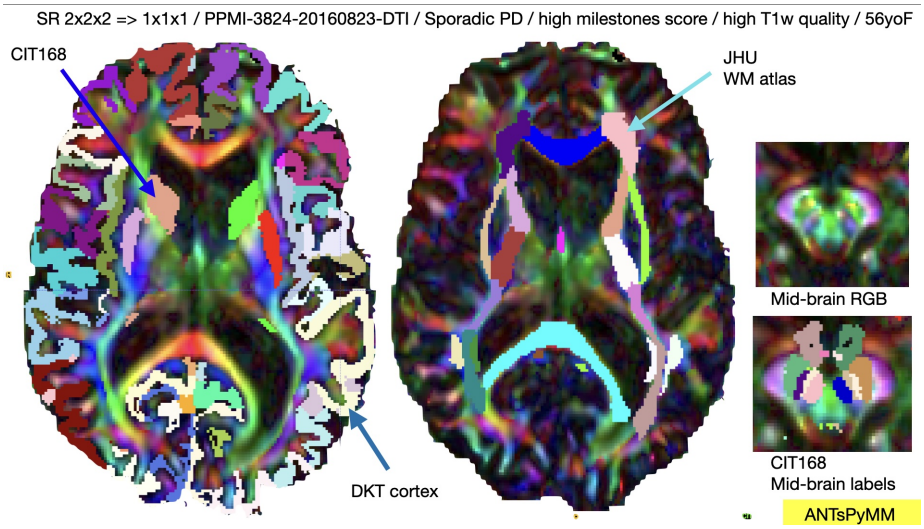

Figure 5: Example SR processing for DTI highligting the multiple coordinate systems to aid interpretation.

compute both functional activity and correlation maps utilizing the recently proposed homotopic labels to delineate major network systems (Yan et al. 2023). The methodology described below is grounded in contemporary understanding of resting-state fMRI analysis and incorporates recommendations from seminal works regarding optimal preprocessing for minimizing motion artifacts and other sources of noise (Shirer et al. 2015; Parkes et al. 2018). As such, our processing reflects a comprehensive approach to resting-state fMRI IDP extraction for real-world multi-site studies of neurodegenerative disease. Overall, the methods aim to facilitate the reliable extraction of functional connectivity patterns that are consistent with underlying neural mechanisms in PD (Tahmasian et al. 2015; Esposito et al. 2013). Similar to the DWI processing, the procedure accepts either a single image or a pair of images with reversed phase encoding direction. The steps are outlined in Figure 6:

1. **Input Preparation**: Inputs include the raw BOLD fMRI time-series data, a reference volumetric subject-specific fMRI template (automatically generated), and T1-weighted anatomical images all from the same subject. These inputs are foundational for aligning functional data with anatomical landmarks and for ensuring that subsequent analyses are anatomically informed. By default, the input fMRI is upsampled to 3mm isotropic resolution and 8 initial volumes are discarded to allow for both signal and subject stabilization.

2. **Preprocessing**: Initial steps include motion correction, application of a despiking algorithm (a `python` implementation of AFNI's 3dDespike (Cox 2012)), and anatomical registration to align the fMRI data with the

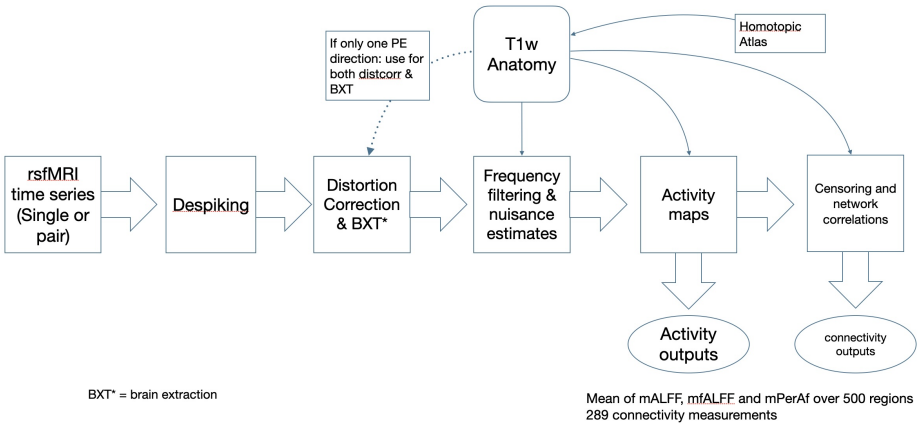

Figure 6: Overview of the rsfMRI processing pipeline based on ANTsX.

T1-weighted image. If a pair of images is passed, these same preprocessing steps are applied and results are concatenated along the time axis.

3. **Noise Reduction**: Anatomical CompCor (aCompCor) is used to mitigate physiological and other noise sources. This is based on recommendations from studies examining the impact of preprocessing strategies on functional connectivity (Shirer et al. 2015; Parkes et al. 2018).

4. **Band-pass Filtering and activity calculation**: The application of a specific frequency range for filtering aligns with recommendations from both Shirer et al. (2015) and Parkes et al. (2018), emphasizing the importance of selecting appropriate frequency bands for resting-state analysis. The default frequency bands are based on empirical evaluation studies described below.

5. **Censoring**: Select volumes are censored based on both motion-based and intensity-based outlier detection. The parameters for this stage derive from empirical evaluation studies on public data as discussed below. Both *censored* and *imputed* versions of the time series are created. A summary of censoring results is recorded in several ways but perhaps most relevant are the variables `*minutes_original_data` and `*minutes_censored_data` which provides the length in minutes of the original versus processed data.

6. **Network Correlation Analysis**: This step involves calculating correlation matrices for identified resting-state networks, utilizing labels described above. Both inter and intra-network correlation values are computed for each of the sub-networks provided by the homotopic parcellation.

7. **Functional activity**: is computed with three models: mfALFF, mALFF and mPerAf as described in (Jia et al. 2020). These are versions of fALFF, ALFF and PerAf where each is divided by the global mean in the brain.

Summary values are averaged within each of 500 labels in the homotopic label set which facilitates left/right asymmetry and mean values which are critical to studying diseases with laterality effects.

Due to the relatively diverse needs of researchers and the variety of rsfMRI that is generally present in public data, we run the above processing with three different sets of parameters. These sets are named by their position in the parameter search data frame as 122, 134 and 129. They encode 3 different choices for outlier rejection (based on motion) and control of nuisance signal via aCompCor. These three parameter choices led to rsfMRI IDPs that were the top performers in terms of reliability and predictive power out of 78 that we tested empirically. See this repository and the technical validation section for further details. IDPs from the rsfMRI processing are denoted by prefixes `rsfMRI_fcnxpro122` for 122 and similarly for 129 and 134.

Dimensionality reduction with SiMLR

Statistical power in cohorts with diverse composition may be challenged by the number of individual predictors (here, 1178). To address this, we adopt similarity-driven multi-view linear reconstruction (SiMLR) for dimensionality reduction and apply the default settings recommended in prior work (B. B. Avants, Tustison, and Stone 2021; Stone et al. 2023). SiMLR provides a reduced number of predictors by creating "sparse feature sets" that are linked across modalities, allowing for their combined use in joint prediction models. As an unsupervised method, SiMLR identifies a joint low-dimensional space that captures the common variability across these diverse modalities. This enables integrated analyses of MRI and acquired non-imaging data (represented as standard tabular outcomes) within the analytical framework of classical regression. Importantly, this approach can be applied even when only a subset of the variables is present.

Here, the SiMLR decomposition is trained in ADNI subjects and subsequently applied to PPMI thereby decoupling the learning and inference stages. Six matrices were decomposed into 100 joint components. The matrices included one for tabular clinical data and five for neuroimaging including T1w related measurements averaged across left and right, T1w related asymmetry measurements, DTI related measurements averaged across left and right, DTI related asymmetry measurements and resting state connectivity measurements. Although cognition and functionally related clinical scores were employed during decomposition, these were not retained for further application to PPMI. The technical validation section will demonstrate how these learned patterns may be used in analyses integrating PPMI IDPs and clinically relevant metrics both cross-sectionally and longitudinally.

Data Records

The PPMI IDPs for T1w, rsfMRI and DTI are located at (B. Avants 2024). The neuroimaging and associated standard PPMI demographics and clinical data is hosted in the LONI Imaging Data Archive (LONI IDA). The former is stored in DICOM format and the latter in tabular `csv` format. Additionally, data dictionaries describing all non-imaging column headers are available on the LONI IDA.

We attach the neuroimaging IDPs to the PPMI Curated Data Cut (v.2024-01-29 `PPMI_Curated_Data_Cut_Public_20240129`) from the LONI IDA. Code for this merging process is within the subtyper package specifically the function merge_ppmi_imaging_clinical_demographic_data. The M3RI IDPs are described in detail here and are in a data table within the `ANTsPyMM` repository (csv format). The full tabular IDPs for both OR and SR outputs are at this location.

We supplement these PPMI data with subjects from ADNI due to the current dearth of control longitudinal neuroimaging in PPMI. As with PPMI, we attach ANTsPyMM IDPs to `ADNIMERGE_10Feb2024` using the `subtyper` function `merge_ADNI_antspymm_by_closest_date`. Select subjects from ADNI are considered for merging with PPMI if they are not diagnosed wtih Alzheimer's disease or mild cognitive impairment (MCI) and have acceptable quality neuroimaging. The ADNI cohort is significantly older (mean of 72.3 years versus 63.9 in PPMI).

We also train a regression model on the matched subjects to adjust imaging variables for systematic differences dut to study populations (ADNI vs PPMI), MRI manufacturers ('GE', 'Philips', 'Siemens') and magnetic field strength. Control subjects aged between 50 and 70 are designated as training samples. The regression map is learned and applied to each IDP throughout the full cohort using the `subtyper` function `adjustByCovariates`. The purpose of this process is to mitigate the influence of different imaging protocols, ensuring that subsequent analyses are less confounded by these factors. This approach has been used in practical studies of ADNI MRI data (Risacher et al. 2017). These merged and adjusted IDP data records are included in the file `ppmi_idps_trim_v1.4.0_SRF.csv`. SiMLR derived variables are denoted `t1PC*` (left-right averaged T1w derived feature sets), `t1aPC*` (asymmetry-related T1w derived feature sets), `dtPC*` (left-right averaged DTI derived feature sets), `dtaPC*` (asymmetry-related DTI derived feature sets) and `rsfPC*` (resting connectivity) where the `*` varies from 1 to 100. These SiMLR derived variables limit the multiple testing considerations to 100 variables because these are typically grouped together. That is, a given PC set (referred to as $simIDP_i^k$) is included in a single model (e.g. if $k = 1$, then $age \approx t1PC1 + t1aPC1 + dt1PC1 + dtaPC1 + rsfPC1$) where $simIDP_1 = t1, simIDP_2 = t1a$, etc. We use this approach in a technical validation section below.

Technical Validation

Components of technical validity that are critical for quantitative methodology in neuroimaging include: (a) generally robust performance across modalities; (b) multi-site reproducibility; (c) disease-specific discrimination from controls in particular over time in the clinical trial setting; (d) sensitivity to or relationship with changes in clinically relevant symptoms at baseline and/or over time. We provide evidence that the current IDPs satisfy these properties in the following sections.

- We quantify reproducibility and reliability in each modality through analysis of three traveling subject cohorts (addressing (a) and (b) above). These cohorts collect imaging data at different sites from the same individuals. Reliability data based on such cohorts are highly relevant for multisite trials which are always impacted by site-specific variation. By aggregating data from the traveling subject cohorts, we offer precise, reproducible reliability estimates (via intra-class correlation) manifested across different scanner types and imaging modalities.
- We derive effect sizes from statistical models that test established hypotheses comparing biomarker classified PD subjects versus control subjects. These show expected effects of PD are detectable in these data. This addresses (c) above.
- We finalize the technical validity section with examples of how scientists may relate IDP measures of brain health to rate of symptom change in PD in a multiple modality (integrative) context. This addresses (d) above.

The scale of the current data supports control for a subset of important PD relevant covariates including disease duration, educational level, sex, age and levodopa dose equivalent daily dose (LEDD). These variables are included in reference models with additional details below.

Robust performance

The technical validity of these methods is supported by previous work, including various open quantitative MRI analysis challenges (Menze et al. 2015; Murphy et al. 2011; Baheti et al. 2021) that span modalities and organ systems. The foundational methods also support applications to non-human data (Allan Johnson et al. 2019; Hopkins and Avants 2013). Furthermore, the consistency of the methodology naturally enables multivariate statistical inference and/or prediction (Stone et al. 2023) even within the multi-study context (Dadu et al. 2024).

Multi-site reproducibility

Traveling subject studies involve scanning the same subjects on multiple MRI scanners at different locations. These studies help in assessing consistency and/or

agreement of image quantification where the only variables are the machines themselves. This is crucial for understanding power in multi-site studies of natural history or intervention and for ensuring that the observed changes in brain structure or function are due to actual physiological changes rather than variations in the imaging process itself.

In this study, we employ traveling cohort data (Hawco et al. 2022; Tanaka et al. 2021; Tong et al. 2019) to assess the agreement of IDPs pooled across multiple sites for the purposes of statistical inference. These data will establish expectations of repeatability for T1w, DTI and rsfMRI as measured by ANTsPyMM processing and are described briefly here:

1. the SRPBS Traveling Subject MRI Dataset (Tanaka et al. 2021):

- 9 healthy subjects travel to 12 sites to be imaged;
- of the 12 sites, 9 have consistently available T1w and rsfMRI in 6 subjects.

2. traveling subject DTI cohort (Tong et al. 2019):

- 3 healthy subjects travel to 4 sites to be imaged;
- T1w and multi-shell DWI/DTI are available.

3. Hawco's traveling subject MRI dataset (Hawco et al. 2022) is available here:

- 4 healthy male subjects travel to 6 sites to be imaged with T1w, rsfMRI and DTI.

Thus, we use these data to characterize the consistency and reliability of these tools when applied to data that has known systematic biases due to site and scanner differences. The results confirm that findings and conclusions drawn from ANTsPyMM are reliable and not overwhelmed by scanner-specific differences or inconsistencies. This knowledge is critical for a foundational framework such as ANTsX/ANTsPyMM upon which scientific studies, machine learning platforms and other methodological comparisons are based. These cohorts represent variability in both MRI manufacturer and MRI model (high variability) that would exceed standard (within-scanner, within-site) test-retest analysis. Results therefore provide a lower-bound on reliability; i.e. within-site (e.g. longitudinal) studies would be expected to have higher reliability in general.

We employ the intra-class correlation to assess results. ICC ranges may be interpreted as (Koo and Li 2016):

- below 0.50: poor
- between 0.50 and 0.75: moderate
- between 0.75 and 0.90: good
- above 0.90: excellent

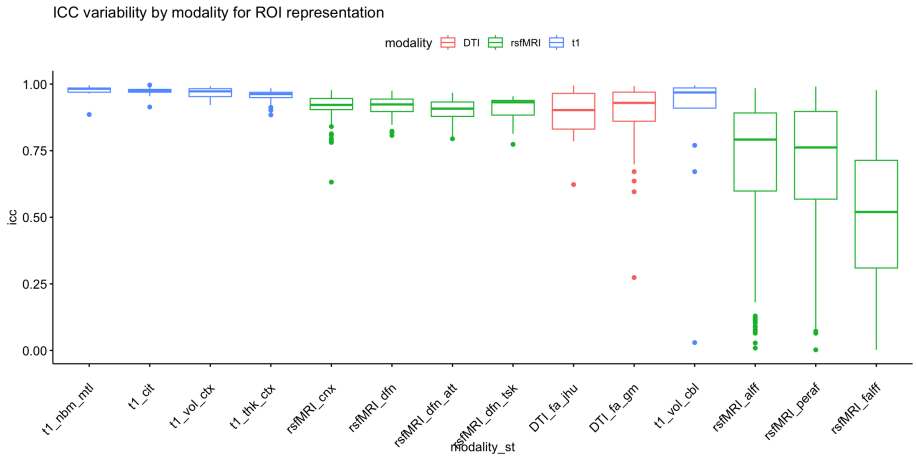

Figure 7: Summary reproducibility results from aggregated traveling subject data. T1 IDPs represent high reproducibility in all categories (cerebellum, CIT168, cortical volume, cortical thickness, basal forebrain and medial temporal lobe). DTI IDPs are also highly reproducible with FA in the cortical gray matter (gm) nearly equaling that of major white matter regions in the JHU atlas. Resting state connectivity shows good to excellent reproducibility; PerAF, fALFF and ALFF are relatively less reproducible – on average – though variability across regions is also high.

We find that ANTsPyMM IDPs derived from the same subjects imaged at different sites with MRI from various manufacturers show overall good to high reliability with a few exceptions within resting state derivatives (fALFF specifically). This provides empirical evidence that multiple modality MRI may be used to derive quantitative phenotypes on which predictive models may be based. Statistical control for site effects should still be applied at the population level using, for example, random effects. The data and code for reproducing these results is available in this location. Figure 7 shows the key summary output for this ICC comparison.

Diagnostic effects in pre-defined structural, white matter and resting functional measurements

Table 2. PD IDPs in ANTsPyMM: T1w L/R average and asym.

IDP	anat
t1.vol.sup.parietal.ctx	Superior Parietal Cortex
t1.vol.inf.parietal.ctx	Inferior Parietal Cortex
t1.vol.paracent.ctx	Paracentral Cortex
t1.vol.postcent.ctx	Postcentral Cortex
t1.vol.precent.ctx	Precentral Cortex
t1.vol.sncdp.	Substantia Nigra Compacta
t1.vol.bn.str.pudp.	Basal Nucleus Striatum, Putamen
t1.vol.bn.gp.gpidp.	Globus Pallidus Internal Segment
t1.vol.bn.gp.gpedp.	Globus Pallidus External Segment
t1.vol.nbm.antbf	Nucleus Basalis Meynert, Anterior Basal Forebrain
t1.vol.nbm.midbf	Nucleus Basalis Meynert, Middle Basal Forebrain
t1.vol.nbm.posbf	Nucleus Basalis Meynert, Posterior Basal Forebrain
t1.vol.dg.ca3mtl	Dentate Gyrus, CA3 Region of Medial Temporal Lobe
t1.midbrain.pons.ratio	Midbrain Pons ratio

Table 3. PD IDPs in ANTsPyMM: DTI L/R average and asym for both fractional anisotropy (FA) and mean diffusion (MD) (not shown).

IDP	anat
dti.fa.sup.l.fasc	Superior Longitudinal Fasciculus FA
dti.fa.deep.snc	Deep Substantia Nigra Compacta FA
dti.fa.snc	Substantia Nigra Compacta FA
dti.fa.sup.cor.rad	Superior Corona Radiata FA
dti.fa.fornixlravg	Fornix FA
dti.fa.ant.int.cap	Anterior Internal Capsule FA
dti.fa.ext.cap	External Capsule FA
dti.fa.post.int.cap	Posterior Internal Capsule FA
dti.fa.rent.int.cap.	Retrolenticular Part of Internal Capsule FA
dti.fa.sup.frnt.occ.fasc	Superior Frontal-Occipital Fasciculus FA
dti.fa.deep.bn.str.pu	Deep Basal Nucleus Striatum, Putamen FA
dti.fa.bn.str.pu	Basal Nucleus Striatum, Putamen FA

Table 4. PD IDPs in ANTsPyMM: rsfMRI bilateral inter or intra-network connectivity (Yan, et. al. homotopic parcellation nomenclature).

IDP	connectivity
rsf.p2.sommotb.2.temppar	Temporal Parietal Region
rsf.p2.sommotb.2.contc	Control Network Component C
rsf.p2.sommotb.2.contb	Control Network Component B
rsf.p2.sommotb.2.conta	Control Network Component A
rsf.p2.sommotb.2.sommotb	Somatomotor Area B
rsf.p2.sommotb.2.sommota	Somatomotor Area A
rsf.p2.sommotb.2.visperi	Peripheral Visual Area
rsf.p2.sommotb.2.viscent	Central Visual Area
rsf.p2.sommotb.2.striatum	Striatum
rsf.p2.sommotb.2.dopamine	Dopaminergic system
rsf.p2.sommotb.2.basalganglia	Basal Ganglia
rsf.p2.sommotb.2.midbrain	Midbrain
rsf.p2.sommota.2.temppar	Temporal Parietal Region
rsf.p2.sommota.2.contc	Control Network Component C
rsf.p2.sommota.2.contb	Control Network Component B
rsf.p2.sommota.2.conta	Control Network Component A
rsf.p2.sommota.2.sommotb	Somatomotor Area B
rsf.p2.sommota.2.sommota	Somatomotor Area A
rsf.p2.sommota.2.visperi	Peripheral Visual Area
rsf.p2.sommota.2.viscent	Central Visual Area
rsf.p2.sommota.2.striatum	Striatum
rsf.p2.sommota.2.dopamine	Dopaminergic system
rsf.p2.sommota.2.basalganglia	Basal Ganglia
rsf.p2.sommota.2.midbrain	Midbrain

Sensitivity to differences from controls

Symptoms of Parkinson's disease (PD) exhibit heterogeneity both across individuals and within a single patient over time. MRI is suited to objective *in vivo* characterization of the neural basis of these changes longitudinally with a variety of structural and functional measurements. Here, we assess longitudinal and cross-sectional effect sizes in T1w, DTI and rsfMRI IDPs that are pre-defined for PD relevance. These regions are listed in Table 2 (T1w), Table 3 (DTI) and Table 4 (rsfMRI) and span motor, associative and limbic systems that may be impacted in PD and associated disorders (Ryman and Poston 2020). These include motor and parietal cortex (Filippi et al. 2020; Sokołowski et al. 2024), midbrain and striatal regions and basal forebrain (Batzu et al. 2023) from T1w. Due to known concomitant, AD-related pathology in some PD subjects, we also include a medial temporal lobe IDP (Das, Hwang, and Poston 2019). Relatedly, we select mean diffusion and FA derived from DTI in the striatum and substantia nigra (Hu et al. 2023) as well as major white matter tracts (Gattellaro et al. 2009; Pietracupa et al. 2018), the fornix and external and internal capsule; a recent large-scale study demonstrated sensitivity of these measures to PD (Owens-Walton et al. 2024). Interestingly, DTI metrics in early PD –

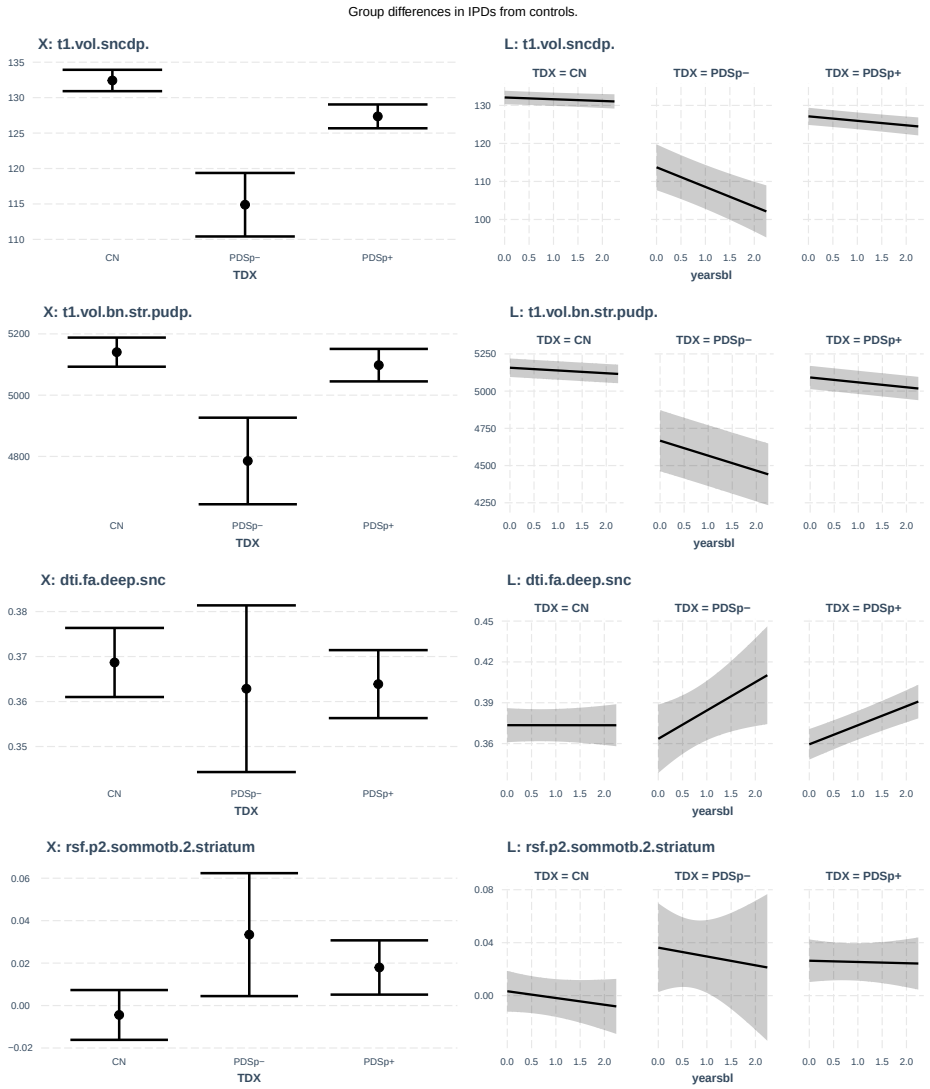

Figure 8: Partial regression plots for example significant IDPs illustrate the trends of differences from controls. The bar plots at left show 95 percent confidence intervals along with estimated means for each group. The line plots at right show the estimated change over time (0 to 4 years) along with 95 percent confidence intervals. Table 5 and 6 detail the associated significance levels and effect sizes.

within both the current study and the recent worldwide study (Owens-Walton et al. 2024) – appear to trend in directions that are opposite to that of other neurodegenerative diseases which provides an interesting opportunity for future work and more nuanced stage-based statistical modeling. In rsfMRI, we focus on connectivity between sensorimotor regions and other networks, in particular visual and cognitive control (Caspers et al. 2021; Wang et al. 2021; Tahmasian et al. 2015). In total, we test 99 different measurements which include left-right averaged as well as asymmetry metrics:

$$avg(x_l, x_r) = \frac{1}{2}(x_l + x_r); \quad asym(x_l, x_r) = |x_l - x_r|$$

derived from those regions which are bilateral. This strategy is a generalizable way of testing laterality effects across all groups, including those without an established dominant side of disease (controls and pre-symptomatic PD subjects).

We provide exemplar linear mixed-effects models (LMMs) that seek to elucidate the complex relationships between neuroimaging biomarkers and the progression of Parkinson's Disease (PD). The analytical framework was constructed using the `R` programming environment, leveraging the `lme4` package (Kuznetsova, Brockhoff, and Christensen 2017; Bates et al. 2014). This methodology allows for the exploration of hierarchical data structures commonly encountered in longitudinal neuroimaging studies, where multiple observations per subject are standard. These models were designed to investigate differences between biomarker-confirmed PPMI PD groups and controls. We accentuate that these models are for demonstration only and do not constitute fully-vetted "official" PPMI results. While these models may not account for all relevant covariates, they do provide evidence of validity by confirming the sensitivity of these IDPs to diagnostic group differences. These models are of the form:

$$\begin{aligned} \text{IDP} \approx\ & (1|ID) + (1|Site) + \text{BV}_{\text{bl}} + Edu + duration_{\text{yrs}} + \\ & modality\_specific\_covariates + age_{\text{bl}} + \\ & Sex_{\text{bio}} + years_{\text{bl}} * \text{DX} \end{aligned}$$

where IDP is the imaging outcome, ID is a random effect for subject ID, $Site$ is a random effect for data collection site, BV_{bl} is baseline brain volume, Edu is educational attainment and $modality\_specific\_covariates$ covaries for modality-specific variability due to site and related effects. Age at baseline and biological sex are additional covariates. The primary predictors of interest are $years_{\text{bl}} * \text{DX}$ i.e. the interaction between time from baseline of the IDP measurement (in years) and the diagnostic group which includes SAA positive and negative PD subjects in addition to controls and MCI. The cross-sectional/longitudinal sample sizes and results for each group within the DX variable are denoted in Table 5 (cross-sectional) and 6 (longitudinal) where a postfix of ".x" indicates a cross-sectional estimate and ".y" a longitudinal one. The columns `anv.x` and `anv.y` reflect

omnibus model p-values; `d` indicates effect size for the corresponding group either cross-sectionally or longitudinally. The `sig` column indicates whether the corrected p-value survives family-wise error (fwe) or false discovery rate (fdr) correction. In the longitudinal cohort, subjects are required to have two or more visits.

Cross-sectional models used standard linear regression (`lm` in `R`) with the same structure as described above but without random effects. Linear mixed-effects models (LMMs) were constructed using the `lmer` function from the `lme4` package and fitted to the data. This process included the standardization of variables within the equation, a critical step given the varying scales and distributions of neuroimaging metrics. Comparative model analysis was conducted to ascertain the significance of various predictors, employing the `anova` function to contrast models with and without DX and the interaction between DX and $years_{\text{bl}}$. This `anova` assesses the "omnibus" model improvement due to the joint addition of both DX and the interaction between DX and $years_{\text{bl}}$. As we are only reporting high level results here, we do not investigate p-values within individual diagnostic groups. These results are shown in Table 5 (for the DX term) and Table 6 (for the longitudinal term). Effect sizes (d.x and d.y) for each term are estimated from the $t-$value and degrees of freedom for each cross-sectional and longitudinal model. Very small effect sizes are those with absolute value less than 0.2. The effects of DX on these IDPs are visualized through predictor effect plots (Larsen and McCleary 1972; Fox and Weisberg 2018) of diagnosis by time generated for each diagnostic category as in Figure 8. These IDPs are significant under family wise error (fwe) multiple comparisons correction at p-value ≤ 0.05 (after correction based on the above-mentioned `anova`). These plots and other regression plots are displayed with the `R` packages `jtools` and `interactions`.

Baseline IDP to longitudinal MDS-UPDRS effects in structural, white matter and resting functional measurements

We use LMMs to estimate the relationship of IDP values to clinical observations as evaluated by MDS-UPDRS 1, 2, 3 (off), total (off) and related scores. While these clinical measurements have well-documented limitations in terms of reliability and interpretability (on behalf of the Parkinson's Progression Markers Initiative et al. 2023), they are consistently available in PPMI. These exemplar assessments differ from the prior section in that they focus only on PPMI subjects as these measurements are absent in ADNI. These models are of the form:

$$\begin{aligned}\text{UPDRSX}_{delta} \approx (1|ID) + \text{UPDRSX}_{bl} + \text{BV}_{\text{bl}} + Edu + LEDD + \\ age_{\text{bl}} + Sex_{\text{bio}} + years_{\text{bl}} * (\sum_{i=1}^{5} simIDP_i^k)\end{aligned}$$

The outcome is UPDRSX_{delta} indicating change in a given MDS-UPDRS score. The majority of these variables are as defined previously. However, we introduce

Table 5. Time independent group effects in PPMI/ADNI. Top-k per modality.

voi	n.x (CN,Sp-,Sp+)	anv.x	d.x.Sp-	d.x.Sp+	sig.x	sig.y
t1.vol.bn.str.pudp.	747/44/574	p = 6.4813e-06	-0.27	-0.08	fwe.x	fwe.y
t1.midbrain.pons.ratio	747/44/574	p = 6.6242e-08	-0.23	-0.26	fwe.x	fwe.y
t1.vol.sncdp.	747/44/574	p = 2.2643e-16	-0.41	-0.30	fwe.x	fwe.y
t1.vol.bn.gp.gpidp.	747/44/574	p = 4.5784e-18	-0.47	0.05	fwe.x	fdr.y
t1.vol.bn.gp.gpe.asymdp.	747/44/574	p = 3.6180e-07	0.29	0.13	fwe.x	fdr.y
t1.vol.bn.gp.gpi.asymdp.	747/44/574	p = 2.0369e-06	0.27	-0.01	fwe.x	fdr.y
t1.vol.bn.str.pu.asymdp.	747/44/574	p = 7.2291e-22	0.54	0.04	fwe.x	n.s.
t1.vol.bn.gp.gpedp.	747/44/574	p = 4.1291e-17	-0.33	0.27	fwe.x	n.s.
t1.vol.snc.asymdp.	747/44/574	p = 0.0004	0.21	0.01	fwe.x	n.s.
t1.vol.nbm.midbf	747/44/574	p = 0.0002	-0.23	-0.06	fwe.x	n.s.
t1.vol.nbm.antbf	747/44/574	p = 0.0022	-0.18	0.01	fdr.x	n.s.
dti.mean.md.snc	327/29/365	p = 0.0002	0.07	0.31	fwe.x	fwe.y
dti.mean.md.deep.snc	327/29/365	p = 0.0005	0.06	0.29	fwe.x	fwe.y
dti.fa.bn.str.pu	327/29/365	p = 0.0029	0.02	-0.24	fdr.x	fdr.y
rsf.p2.sommotb.2.striatum	327/26/277	p = 0.0035	0.20	0.23	fdr.x	n.s.

Table 6. Longitudinal group effects in PPMI/ADNI. Top-k per modality.

voi	n.y (CN,Sp-,Sp+)	anv.y	d.y	d.y.Sp-	d.y.Sp+	sig.y	sig.x
t1.vol.bn.str.pudp.	422/20/286	p = 1.4056e-11	-0.56	-0.48	-0.28	fwe.y	fwe.x
t1.midbrain.pons.ratio	422/20/286	p = 0.0002	-0.15	-0.23	-0.23	fwe.y	fwe.x
t1.vol.sncdp.	422/20/286	p = 0.0005	-0.14	-0.27	-0.13	fwe.y	fwe.x
t1.vol.bn.gp.gpidp.	422/20/286	p = 0.0018	-0.40	-0.26	0.04	fdr.y	fwe.x
t1.vol.bn.gp.gpe.asymdp.	422/20/286	p = 0.0066	-0.01	0.23	0.04	fdr.y	fwe.x
t1.vol.dg.ca3mtl	422/20/286	p = 0.0144	-0.58	-0.10	0.18	fdr.y	n.s.
t1.vol.bn.gp.gpi.asymdp.	422/20/286	p = 0.0156	0.04	0.21	-0.03	fdr.y	fwe.x
dti.fa.sup.cor.rad	158/18/250	p = 1.9327e-05	0.01	0.33	0.39	fwe.y	n.s.
dti.mean.md.snc	158/18/250	p = 4.5422e-05	0.07	-0.30	-0.39	fwe.y	fwe.x
dti.fa.rent.int.cap.	158/18/250	p = 8.8642e-05	0.05	0.35	0.32	fwe.y	n.s.
dti.mean.md.deep.snc	158/18/250	p = 0.0001	0.05	-0.25	-0.38	fwe.y	fwe.x
dti.fa.sup.l.fasc	158/18/250	p = 0.0001	0.06	0.30	0.35	fwe.y	n.s.
dti.fa.ant.int.cap	158/18/250	p = 0.0003	-0.03	0.31	0.31	fwe.y	n.s.
dti.mean.md.sup.cor.rad	158/18/250	p = 0.0004	-0.01	-0.28	-0.33	fwe.y	n.s.
dti.fa.fornixlravg	158/18/250	p = 0.0004	-0.07	0.24	0.34	fwe.y	n.s.
dti.mean.md.ant.int.cap	158/18/250	p = 0.0006	0.04	-0.30	-0.30	fwe.y	n.s.
dti.mean.md.sup.frnt.occ.fasc	158/18/250	p = 0.0008	0.06	-0.27	-0.31	fwe.y	n.s.
dti.mean.md.sup.l.fasc	158/18/250	p = 0.0010	-0.08	-0.28	-0.29	fwe.y	n.s.
dti.mean.md.fornixlravg	158/18/250	p = 0.0011	0.03	-0.22	-0.33	fwe.y	n.s.
dti.fa.deep.snc	158/18/250	p = 0.0013	-0.00	0.20	0.34	fwe.y	n.s.
dti.mean.md.post.int.cap	158/18/250	p = 0.0024	0.00	-0.24	-0.29	fdr.y	n.s.
dti.mean.md.rent.int.cap.	158/18/250	p = 0.0025	-0.05	-0.26	-0.27	fdr.y	n.s.
dti.fa.snc	158/18/250	p = 0.0033	-0.02	0.16	0.32	fdr.y	n.s.
dti.mean.md.ext.cap	158/18/250	p = 0.0036	0.00	-0.26	-0.26	fdr.y	n.s.
dti.fa.bn.str.pu	158/18/250	p = 0.0039	-0.08	0.25	0.26	fdr.y	fdr.x
dti.mean.md.deep.bn.str.pu	158/18/250	p = 0.0045	-0.02	-0.27	-0.24	fdr.y	n.s.
dti.mean.md.bn.str.pu	158/18/250	p = 0.0050	-0.02	-0.26	-0.24	fdr.y	n.s.

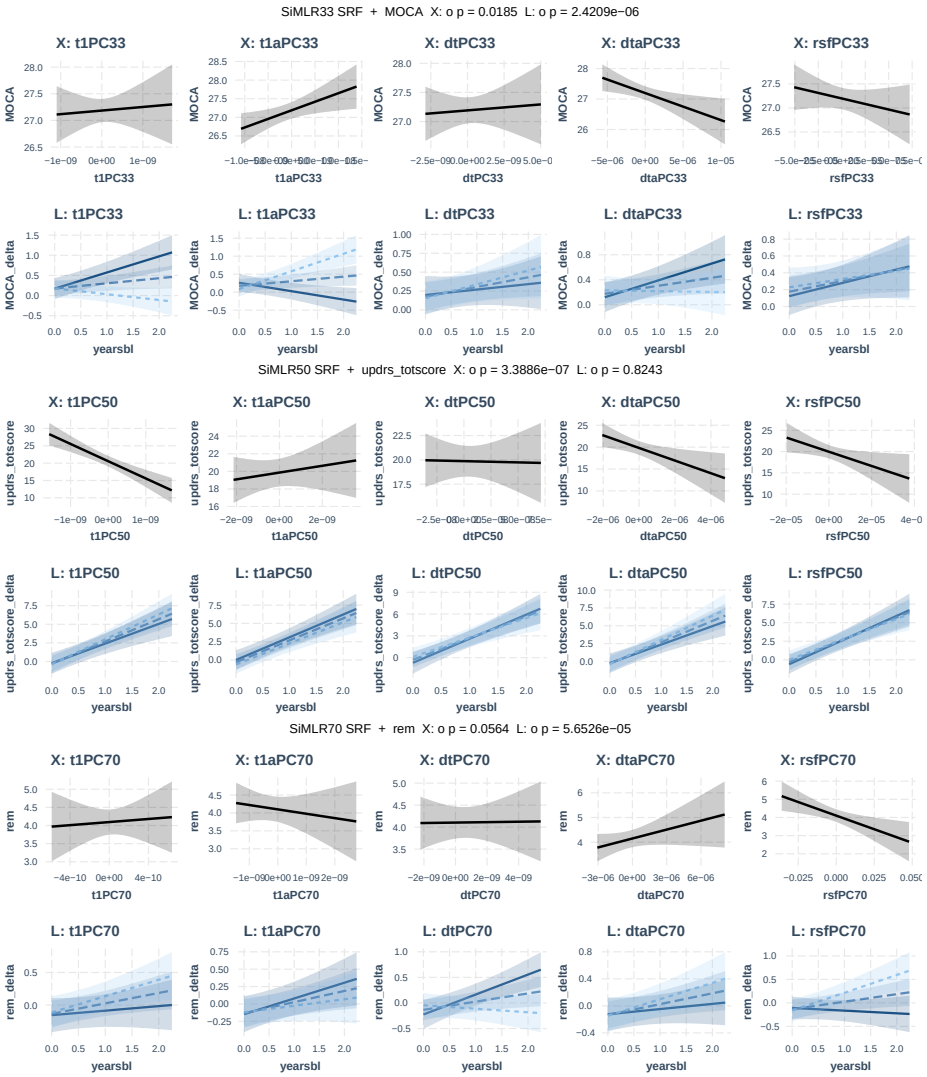

Figure 9: Select predictor effect plots for SiMLR mapping between M3RI and PD symptomology. Plots headed with "X" relate to cross-sectional effects while "L" is longitudinal. Significance for the class of effects is also noted in the main title of each figure pair ("p = ..."). Shaded regions in all panels show 95 percent confidence intervals. In the "L" plots, the predictor effect plots visualizes interaction between time from baseline and the given SiMLR IDP. The darker lines indicate the relationship of higher values in the given imaging score with the change in the outcome. Lighter dashed lines indicate the relationship of lower values in the given imaging score with the change in the outcome. For example, higher values in t1PC33 are associated with MOCA preservation over time (or increased learning) as is decreased asymmetry. The SiMLR50 plots (middle panels) show robust cross-sectional association with total score but no evidence of longitudinal association. The SiMLR70 plots (bottom pair) show association of both DTI and resting state IDPs with REM sleep disturbance changes over time.

Table 7. Significant SiMLR IDP to clinical measurements: (up to) top five for each score.

cog	voi	n.x	n.y	anv.x	anv.y	d.x	d.y	S.m1.1	S.m2.1	sig
MOCA	33	1032	346	p = 0.0185	p = 2.4209e-06	0.16	0.55	t1.thk.asym.parahippocampal.ctx	t1.thk.isthmus.cingulate.ctx	fwe
MOCA	72	1032	346	p = 0.0385	p = 0.0002	0.16	0.32	rsf.p2.salventattnb.2.striatum	dti.fa.asym.sup.frontal	fdr
MOCA	60	1032	346	p = 0.0463	p = 0.0006	0.15	0.31	t1.thkasymviibcerebellum	rsf.p2.defaulta.2.defaultc	fdr
MOCA	98	1032	346	p = 0.2848	p = 0.0007	0.14	0.34	dti.fa.asym.isthmus.cingulate	NA	fdr
MOCA	57	1032	346	p = 0.4910	p = 0.0006	0.10	0.24	rsf.p2.dorsattna.2.limbicb	dti.fa.post.int.cap.asym	fdr
pigd	50	1002	314	p = 0.0008	p = 0.0016	0.28	0.38	t1.thk.sncdp.	NA	fdr
pigd	71	1002	314	p = 0.3645	p = 0.0001	0.10	0.43	t1.thkasymcrus.icerebellum	rsf.p2.dorsattnb.2.dorsattnb	fdr
pigd	55	1002	314	p = 0.1774	p = 0.0006	0.15	0.31	dti.fa.inf.frnt.occ.fasciculus.asym	t1.vol.rostral.ant.cingulate.ctx	fdr
pigd	18	1002	314	p = 0.2038	p = 0.0009	0.15	0.23	t1.thk.asym.sup.frontal.ctx	rsf.p2.limbicb.2.dorsattna	fdr
pigd	47	1002	314	p = 0.8463	p = 0.0005	0.07	0.30	t1.vol.fusiform.ctx	rsf.p2.conta.2.sommota	fdr
rem	70	1030	345	p = 0.0564	p = 5.6526e-05	0.17	0.36	dti.fa.ch13	rsf.p2.defaultc.2.conta	fwe
rem	71	1030	345	p = 0.2772	p = 2.0027e-05	0.10	0.42	dti.fa.die.hth	rsf.p2.dorsattnb.2.dorsattnb	fwe
rem	37	1030	345	p = 0.0321	p = 0.0002	0.21	0.35	rsf.p2.contb.2.sommota	dti.fa.corticospinal.tract.asym	fwe
rem	68	1030	345	p = 0.0159	p = 0.0006	0.13	0.31	dti.fa.nbm.pos	rsf.p2.basalganglia.2.limbica	fdr
rem	5	1030	345	p = 0.0608	p = 0.0011	0.14	0.26	dti.fa.bn.gp.gpe.asym	NA	fdr
updrs.totscore	50	980	308	p = 3.3886e-07	p = 0.8243	0.33	0.12	t1.thk.sncdp.	NA	fwe
updrs.totscore	55	980	308	p = 0.0233	p = 3.2863e-05	0.18	0.50	dti.fa.inf.frnt.occ.fasciculus.asym	rsf.p2.defaultc.2.dorsattna	fwe
updrs.totscore	23	980	308	p = 3.5218e-06	p = 0.8743	0.21	0.10	t1.thk.post.cingulate.ctx	dti.fa.nbm.asym.pos	fwe
updrs.totscore	62	980	308	p = 0.0001	p = 0.6615	0.25	0.15	rsf.p2.defaulta.2.basalganglia	t1.thk.snc.asymdp.	fwe
updrs.totscore	4	980	308	p = 0.1119	p = 0.0008	0.15	0.38	rsf.p2.conta.2.dopamine	NA	fdr
updrs1	27	1026	341	p = 0.1107	p = 8.2712e-05	0.14	0.31	dti.fa.bn.gp.vep.asym	t1.volasymxcerebellum	fwe
updrs1	48	1026	341	p = 0.2937	p = 0.0008	0.12	0.25	t1.thk.asym.parahippocampalmtl	dti.fa.bn.str.pu.asym	fdr
updrs2	50	1033	345	p = 0.0002	p = 0.0052	0.28	0.26	t1.thk.sncdp.	NA	fwe
updrs2	55	1033	345	p = 0.0003	p = 0.0324	0.23	0.30	t1.thk.nbm.asym.midbf	NA	fwe
updrs2	62	1033	345	p = 9.9211e-05	p = 0.2060	0.22	0.21	rsf.p2.defaulta.2.basalganglia	t1.thk.snc.asymdp.	fwe
updrs2	36	1033	345	p = 0.0005	p = 0.1851	0.22	0.21	t1.thk.asym.postcent.ctx	t1.midbrain.pons.ratio	fwe
updrs2	76	1033	345	p = 0.0004	p = 0.3169	0.18	0.20	rsf.p2.limbica.2.limbicb	NA	fwe
updrs3	50	992	314	p = 3.2232e-07	p = 0.6948	0.32	0.18	t1.thk.sncdp.	dti.fa.sup.frnt.occ.fasc.asym	fwe
updrs3	4	992	314	p = 0.0676	p = 1.3955e-05	0.13	0.42	rsf.p2.conta.2.dopamine	t1.thk.medial.orbitofrontal.ctx	fwe
updrs3	23	992	314	p = 1.1930e-05	p = 0.1760	0.23	0.22	dti.fa.nbm.asym.pos	t1.vol.nbm.asym.antbf	fwe
updrs3	55	992	314	p = 0.0527	p = 0.0001	0.17	0.45	dti.fa.inf.frnt.occ.fasciculus.asym	rsf.p2.defaultc.2.dorsattna	fwe
updrs3	63	992	314	p = 0.2878	p = 5.8129e-05	0.09	0.44	dti.fa.tapetum.asym	NA	fwe

covariates for treatment effects (Levodopa Equivalent Daily Dose, LEDD) as well as baseline values of the given score. This latter variable approximates a control for subject and domain-specific disease severity. As such, these models are relatively conservative in terms of their attribution of variance to IDP values. The predictor of interest, here, is $years_{\text{bl}} * (\sum_{i=1}^{5} simIDP_i^k)$ which estimates change in the given MDS-UPDRS score (or derived score / subscore) in relation to brain structure (including asymmetry) and function as measured by three modalities. The p-value associated with each of the k in $1 \cdots 100$ models is determined by the amount of additional variance that is explained by the SiMLR IDPs (`R anova` function). We determine significance from the omnibus p-value returned by `anova`. The effect sizes are derived from the single most predictive SiMLR IDP in each model; additional influence by secondary IDPs would augment estimates. These models are assessed in the range of baseline to 2.25 years change. As in the prior section, cross-sectional results are derived with standard regression (`lm`); the outcome in this case, however, is the raw score, not its change.

The effects are visualized, in Figure 9, through effect plots for select IDPs of interest. Effect sizes for each significant (fdr or fwe) pair of outcomes and IDPs in Table 7 where S.m1.1 indicates the top IDP feature contributing to the model. If S.m2.1 is present, this means that a second predictor also contributes significantly to the association (uncorrected $p \leq 0.05$ based on the t-value for a given $simIDP_i^k$ where i indexes the individual type of measurement and k indicates the k^{th} component). The clinical measurement and its most highly weighted IDP is also listed. In several cases, two or more distinct modalities contribute effectively. Moreover, although SiMLR's multivariate feature learning was performed on a separate cohort, several reasonable associations are brought out by this analysis: involvement of hypothalamus FA (`dti.fa.die.hth`) with REM sleep disturbance (rem), connectivity between dopaminergic regions and cognitive control regions (`rsf.p2.conta.2.dopamine`) and MDS-UPDRS-III scores and thickness of substantia nigra pars compacta (`t1.thk.sncdp`) with several measures including postural instability and gait disturbance (PIGD). Recall that we are only reporting, in Table 7, the top features; each $simIDP_i^k$ involves many regions. Region names are described in detail online in the data dictionary and associated documentation.

This SiMLR study demonstrates that brain state – as measured jointly by these modalities – may contribute to acceleration/deceleration of changes in MDS-UPDRS and related scores. However, we accentuate that these models are relatively simple and linear; as such, they yield only rough suggestions that additional modeling effort may be warranted to understand the differential value of these IDPs across the spectrum of PD symptomology. Furthermore, this analysis grouped all PPMI subjects together (excluding controls); as such, it lacks the specificity that may be needed to parse subgroup relationships or those that only occur within specific stages of PD. The subjects comprising these results span a variety of PD-related subgroups: PDGBA: 8 / PDLRRK2: 14 / PDSNCA: 1 / PDSporadic: 367 / ProdromalGBA: 8 / ProdromalLRRK2: 24 / ProdromalSporadic: 533 (median across results for the baseline cohort; the

longitudinal cohort subjects are fewer as they are required to have two or more visits: PDGBA: 6 / PDLRRK2: 7 / PDSporadic: 172 / ProdromalGBA: 7 / ProdromalLRRK2: 16 / ProdromalSporadic: 133). Despite these limitations, Table 7 demonstrates that all three modalities studied here may jointly influence clinical presentation and/or symptoms. Furthermore, several of these models indicate that multiple IDPs are changing in concert with symptom progression.

In summary, these data and reference results demonstrate the potential of multimodal neuroimaging and integrative statistical approaches in PD and neurodegenerative disease research more generally. This tabulated multi-modality MR IDP dataset for PPMI – derived from deeply validated open source methods – represents a valuable opportunity to help standardize as well as advance PD M3RI research. It simplifies – to the extent that is currently possible – the analysis of complex imaging data and potentially accelerates the discovery of novel insights into PD progression and effects. The timing of this data release is critical given the newly available SAA biomarker. Additionally, this methodology holds promise for broader applications, potentially benefiting research into other neurological conditions.

Usage Notes

An example of processing used here is shown in the github respository https://github.com/stnava/ANTPD_antspymm where we combine easily accessible multi-view neuroimaging with our open source methods for demonstration purposes. All images referred to in this research were processed in a style identical to this example.

Code availability

Core image processing was done with `python 3.9` while document creation was achieved with `R` version `4.3.0` – "Already Tomorrow". ANTsPyMM is installable via `pypi` and available at github. The version used for this work is `1.4.0` along with tensorflow `2.11.0`, antspyx `0.5.0`, antspynet `0.2.8` and antspyt1w `0.9.4`. Subtyper `v1.0.0` and ANTsR `0.6.2` contain many utilities used in the creation of this compilable document which was built with Rmarkdown (Xie, Dervieux, and Riederer 2020).

Acknowledgements

Our sincere appreciation to the Michael J. Fox Foundation (MJFF) for supporting this work through MJFF-021144. Technical development for aspects of the software used in this work are supported by the Office of Naval Reseach ONR Award Number: N00014-23-1-2317.

Author contributions statement

B.A. conceptualized and designed the study. L.F., O.H., A.R., A.S., X.W. conducted the experiments and collected the data. B.A. and L.B. performed data analysis and interpretation. N.J.T., J.R.S. and P.A.C. contributed to the development of the software framework and methodology. A.S. and A.R. were responsible for the software and computational tools used in the study. L.C., B.M., R.G, K.P. and K.M. supervised the research and provided critical feedback on the manuscript. B.A. wrote the first draft of the manuscript. All authors reviewed and approved the final version of the manuscript.

Competing interests

BA declares research support and consulting fees from The Michael J Fox Foundation. LMC declares research support and consulting fees from The Michael J Fox Foundation. KP declares consultancies for Curasen; was on a scientific advisory board for Curasen and Amprion; honoraria from invited scientific presentations to universities and professional societies not exceeding $5000 per year from California Congress of Clinical Neurology, California Neurological Society, and Johns Hopkins University; and patents or patent applications numbers 17/314,979 and 63/377,293. KP also declares grants to her institution (Stanford University School of Medicine) from NIH/NINDS NS115114, NS062684, NS075097, NIH/NIA U19 AG065156, P30 AG066515, The Michael J Fox Foundation, Lewy Body Dementia Association, Alzheimer's Drug Discovery Foundation, Sue Berghoff LBD Research Fellowship, and the Knight Initiative for Brain Resilience. KM declares support to his institution (Institute for Neurodegenerative Disorders) from The Michael J Fox Foundation. KM also declares consultancies for Invicro, The Michael J Fox Foundation, Roche, Calico, Coave, Neuron23, Orbimed, Biohaven, Anofi, Koneksa, Merck, Lilly, Inhibikase, Neuramedy, IRLabs, and Prothena. KM participates on DSMB at Biohaven.

References

Allan Johnson, G., Nian Wang, Robert J. Anderson, Min Chen, Gary P. Cofer, James C. Gee, Forrest Pratson, Nicholas Tustison, and Leonard E. White. 2019. "Whole Mouse Brain Connectomics." *Journal of Comparative Neurology* 527 (13): 2146–57. https://doi.org/10.1002/cne.24560.

Aquino, Domenico, Valeria Contarino, Alberto Albanese, Ludovico Minati, Laura Farina, Marina Grisoli, Antonio Elia, Maria Grazia Bruzzone, and Luisa Chiapparini. 2014. "Substantia Nigra in Parkinson's Disease: A Multimodal MRI Comparison Between Early and Advanced Stages of the Disease." *Neurological Sciences* 35 (5): 753–58. https://doi.org/10.1007/s10072-013-1595-2.

Avants, Brian. 2024. "PPMI MR IDPs," March. https://doi.org/10.6084/m9.figshare.25361071.v2.

Avants, Brian B., Jeffrey T. Duda, Emily Kilroy, Kate Krasileva, Kay Jann, Benjamin T. Kandel, Nicholas J. Tustison, et al. 2015. "The Pediatric Template of Brain Perfusion." *Scientific Data* 2 (1): 150003. https://doi.org/10.1038/sdata.2015.3.

Avants, Brian B., R. Matthew Hutchison, Alvydas Mikulskis, Cristian Salinas-Valenzuela, Richard Hargreaves, John Beaver, and Ping Chiao. 2019. "Amyloid Beta–positive Subjects Exhibit Longitudinal Network-Specific Reductions in Spontaneous Brain Activity." *Neurobiology of Aging*. https://doi.org/10.1016/j.neurobiolaging.2018.10.002.

Avants, Brian B., Nicholas J. Tustison, and James R. Stone. 2021. "Similarity-Driven Multi-View Embeddings from High-Dimensional Biomedical Data." *Nature Computational Science* 1 (2): 143–52. https://doi.org/10.1038/s43588-021-00029-8.

Avants, Brian, Nicholas J Tustison, Corey T McMillan, Taylor Gosselin, Roger Gunn, and Jacob Hesterman. 2023. "Concurrent 3D Super Resolution on Intensity and Segmentation Maps Improves Detection of Structural Effects in Neurodegenerative Disease." *medRxiv : The Preprint Server for Health Sciences*. https://doi.org/10.1101/2023.02.02.23285376.

Baheti, Bhakti, Diana Waldmannstetter, Satrajit Chakrabarty, Hamed Akbari, Michel Bilello, Benedikt Wiestler, Julian Schwarting, et al. 2021. "The Brain Tumor Sequence Registration Challenge: Establishing Correspondence Between Pre-Operative and Follow-up MRI Scans of Diffuse Glioma Patients." arXiv. https://doi.org/10.48550/arXiv.2112.06979.

Bates, Douglas, Martin Mächler, Ben Bolker, and Steve Walker. 2014. "Fitting Linear Mixed-Effects Models Using Lme4." arXiv. https://doi.org/10.48550/arXiv.1406.5823.

Batzu, Lucia, Daniele Urso, Michel J. Grothe, Dániel Veréb, K. Ray Chaudhuri, and Joana B. Pereira. 2023. "Increased Basal Forebrain Volumes Could Prevent Cognitive Decline in *LRRK2* Parkinson's Disease." *Neurobiology of Disease* 183 (July): 106182. https://doi.org/10.1016/j.nbd.2023.106182.

Bega, Danny, Phillip H. Kuo, Anastasia Chalkidou, Mariusz T. Grzeda, Thomas Macmillan, Christine Brand, Zulfiqar H. Sheikh, and Angelo Antonini. 2021. "Clinical Utility of DaTscan in Patients with Suspected Parkinsonian Syndrome: A Systematic Review and Meta-Analysis." *NPJ Parkinson's Disease* 7 (May): 43. https://doi.org/10.1038/s41531-021-00185-8.

Calabresi, Paolo, Alessandro Mechelli, Giuseppina Natale, Laura Volpicelli-Daley, Giulia Di Lazzaro, and Veronica Ghiglieri. 2023. "Alpha-Synuclein in Parkinson's Disease and Other Synucleinopathies: From Overt Neurodegeneration Back to Early Synaptic Dysfunction." *Cell Death & Disease* 14 (3): 1–16. https://doi.org/10.1038/s41419-023-05672-9.

Carass, Aaron, Jennifer L. Cuzzocreo, Shuo Han, Carlos R. Hernandez-Castillo, Paul E. Rasser, Melanie Ganz, Vincent Beliveau, et al. 2018. "Comparing Fully Automated State-of-the-Art Cerebellum Parcellation from Magnetic Resonance Images." *NeuroImage* 183 (December): 150–72. https://doi.org/10.1016/j.neuroimage.2018.08.003.

Caspers, Julian, Christian Rubbert, Simon B. Eickhoff, Felix Hoffstaedter, Martin

Südmeyer, Christian J. Hartmann, Benjamin Sigl, et al. 2021. "Within and Across Network Alterations of the Sensorimotor Network in Parkinson's Disease." *Neuroradiology* 63 (12): 2073–85. https://doi.org/10.1007/s00234-021-02731-w.

Cox, Robert W. 2012. "AFNI: What a Long Strange Trip It's Been." *NeuroImage*, 20 YEARS OF fMRI, 62 (2): 743–47. https://doi.org/10.1016/j.neuroimage.2011.08.056.

Dadu, Anant, Michael Ta, Nick Tustison, Ali Daneshmand, Ken Marek, Andrew B. Singleton, Roy H. Campbell, et al. 2024. "Prediction, Prognosis and Monitoring of Neurodegeneration at Biobank-Scale via Machine Learning and Imaging." {SSRN} {Scholarly} {Paper}. Rochester, NY. https://doi.org/10.2139/ssrn.4733955.

Das, Tanusree, Jaclyn J. Hwang, and Kathleen L. Poston. 2019. "Episodic Recognition Memory and the Hippocampus in Parkinson's Disease: A Review." *Cortex* 113 (April): 191–209. https://doi.org/10.1016/j.cortex.2018.11.021.

Dickson, Dennis W., Hiroshige Fujishiro, Carolyn Orr, Anthony DelleDonne, Keith A. Josephs, Roberta Frigerio, Melinda Burnett, Joseph E. Parisi, Kevin J. Klos, and J. Eric Ahlskog. 2009. "Neuropathology of Non-Motor Features of Parkinson Disease." *Parkinsonism & Related Disorders* 15 Suppl 3 (December): S1–5. https://doi.org/10.1016/S1353-8020(09)70769-2.

Disease, Movement Disorder Society Task Force on Rating Scales for Parkinson's. 2003. "The Unified Parkinson's Disease Rating Scale (UPDRS): Status and Recommendations." *Movement Disorders* 18 (7): 738–50. https://doi.org/10.1002/mds.10473.

Droby, Amgad, Moran Artzi, Hedva Lerman, R. Matthew Hutchison, Dafna Ben Bashat, Nurit Omer, Tanya Gurevich, et al. 2022. "Aberrant Dopamine Transporter and Functional Connectivity Patterns in LRRK2 and GBA Mutation Carriers." *Npj Parkinson's Disease* 8 (1): 1–7. https://doi.org/10.1038/s41531-022-00285-z.

Esposito, Fabrizio, Alessandro Tessitore, Alfonso Giordano, Rosita De Micco, Antonella Paccone, Renta Conforti, Giuseppe Pignataro, Lucio Annunziato, and Gioacchino Tedeschi. 2013. "Rhythm-Specific Modulation of the Sensorimotor Network in Drug-Naïve Patients with Parkinson's Disease by Levodopa." *Brain* 136 (3): 710–25. https://doi.org/10.1093/brain/awt007.

Fearnley, Julian M., and Andrew J. Lees. 1991. "Ageing and {Parkinson}'s Disease: Substantia Nigra Regional Selectivity." *Brain* 114 (5): 2283–2301. https://doi.org/10.1093/brain/114.5.2283.

Filippi, Massimo, Elisabetta Sarasso, Noemi Piramide, Tanja Stojkovic, Iva Stankovic, Silvia Basaia, Andrea Fontana, et al. 2020. "Progressive Brain Atrophy and Clinical Evolution in Parkinson's Disease." *NeuroImage: Clinical* 28 (January): 102374. https://doi.org/10.1016/j.nicl.2020.102374.

Fox, John, and Sanford Weisberg. 2018. "Visualizing Fit and Lack of Fit in Complex Regression Models with Predictor Effect Plots and Partial Residuals." *Journal of Statistical Software* 87 (9): 1–27. https://doi.org/10.18637/jss.v087.i09.

Garyfallidis, Eleftherios, Matthew Brett, Bagrat Amirbekian, Ariel Rokem,

Stefan Van Der Walt, Maxime Descoteaux, and Ian Nimmo-Smith. 2014. "Dipy, a Library for the Analysis of Diffusion MRI Data." *Frontiers in Neuroinformatics* 8. https://www.frontiersin.org/articles/10.3389/fninf.2014.00008.

Gattellaro, G., L. Minati, M. Grisoli, C. Mariani, F. Carella, M. Osio, E. Ciceri, A. Albanese, and M. G. Bruzzone. 2009. "White Matter Involvement in Idiopathic Parkinson Disease: A Diffusion Tensor Imaging Study." *American Journal of Neuroradiology* 30 (6): 1222–26. https://doi.org/10.3174/ajnr.A1556.

Gorgolewski, Krzysztof J., Tibor Auer, Vince D. Calhoun, R. Cameron Craddock, Samir Das, Eugene P. Duff, Guillaume Flandin, et al. 2016. "The Brain Imaging Data Structure, a Format for Organizing and Describing Outputs of Neuroimaging Experiments." *Scientific Data* 3 (June): 160044. https://doi.org/10.1038/sdata.2016.44.

Hacker, Carl D., Joel S. Perlmutter, Susan R. Criswell, Beau M. Ances, and Abraham Z. Snyder. 2012. "Resting State Functional Connectivity of the Striatum in Parkinson's Disease." *Brain* 135 (12): 3699–3711. https://doi.org/10.1093/brain/aws281.

Haris, Muhammad, Gregory Shakhnarovich, and Norimichi Ukita. 2020. "Deep Back-Projection Networks for Single Image Super-Resolution." *IEEE Transactions on Pattern Analysis and Machine Intelligence*. https://doi.org/10.1109/tpami.2020.3002836.

Hawco, Colin, Erin W. Dickie, Gabrielle Herman, Jessica A. Turner, Miklos Argyelan, Anil K. Malhotra, Robert W. Buchanan, and Aristotle N. Voineskos. 2022. "A Longitudinal Multi-Scanner Multimodal Human Neuroimaging Dataset." *Scientific Data* 9 (1): 332. https://doi.org/10.1038/s41597-022-01386-3.

Hopkins, William D., and Brian B. Avants. 2013. "Regional and Hemispheric Variation in Cortical Thickness in Chimpanzees (Pan Troglodytes)." *Annals of Internal Medicine*. https://doi.org/10.1523/JNEUROSCI.2996-12.2013.

Hu, Zexuan, Peng Sun, Ajit George, Xiangling Zeng, Mengyan Li, Tsen-Hsuan Lin, Zezhong Ye, et al. 2023. "Diffusion Basis Spectrum Imaging Detects Pathological Alterations in Substantia Nigra and White Matter Tracts with Early-Stage Parkinson's Disease." *European Radiology* 33 (12): 9109–19. https://doi.org/10.1007/s00330-023-09780-0.

Iglesias, Juan Eugenio, Koen Van Leemput, Priyanka Bhatt, Christen Casillas, Shubir Dutt, Norbert Schuff, Diana Truran-Sacrey, Adam Boxer, Bruce Fischl, and Alzheimer's Disease Neuroimaging Initiative. 2015. "Bayesian Segmentation of Brainstem Structures in MRI." *NeuroImage* 113 (June): 184–95. https://doi.org/10.1016/j.neuroimage.2015.02.065.

Jia, Xi-Ze, Jia-Wei Sun, Gong-Jun Ji, Wei Liao, Ya-Ting Lv, Jue Wang, Ze Wang, Han Zhang, Dong-Qiang Liu, and Yu-Feng Zang. 2020. "Percent Amplitude of Fluctuation: A Simple Measure for Resting-State fMRI Signal at Single Voxel Level." *PLOS ONE* 15 (1): e0227021. https://doi.org/10.1371/journal.pone.0227021.

Kim, Jinhee, Marion Criaud, Sang Soo Cho, María Díez-Cirarda, Alexander

Mihaescu, Sarah Coakeley, Christine Ghadery, et al. 2017. "Abnormal Intrinsic Brain Functional Network Dynamics in Parkinson's Disease." *Brain* 140 (11): 2955–67. https://doi.org/10.1093/brain/awx233.

Klein, Arno, and Jason Tourville. 2012. "101 Labeled Brain Images and a Consistent Human Cortical Labeling Protocol." *Frontiers in Neuroscience* 6. https://www.frontiersin.org/journals/neuroscience/articles/10.3389/fnins.2012.00171.

Koo, Terry K., and Mae Y. Li. 2016. "A Guideline of Selecting and Reporting Intraclass Correlation Coefficients for Reliability Research." *Journal of Chiropractic Medicine* 15 (2): 155–63. https://doi.org/10.1016/j.jcm.2016.02.012.

Kuznetsova, Alexandra, Per B. Brockhoff, and Rune Haubo Bojesen Christensen. 2017. "lmerTest Package: Tests in Linear Mixed Effects Models." *Journal of Statistical Software* 82 (13). https://doi.org/10.18637/jss.v082.i13.

Larsen, Wayne A., and Susan J. McCleary. 1972. "The Use of Partial Residual Plots in Regression Analysis." *Technometrics* 14 (3): 781–90. https://doi.org/10.1080/00401706.1972.10488966.

Lee, Virginia M.-Y., and John Q. Trojanowski. 2006. "Mechanisms of Parkinson's Disease Linked to Pathological α-Synuclein: New Targets for Drug Discovery." *Neuron* 52 (1): 33–38. https://doi.org/10.1016/j.neuron.2006.09.026.

Li, Xiangrui, Paul S. Morgan, John Ashburner, Jolinda Smith, and Christopher Rorden. 2016. "The First Step for Neuroimaging Data Analysis: DICOM to NIfTI Conversion." *Journal of Neuroscience Methods* 264 (May): 47–56. https://doi.org/10.1016/j.jneumeth.2016.03.001.

Liu, Alan King Lun, Raymond Chuen-Chung Chang, Ronald K. B. Pearce, and Steve M. Gentleman. 2015. "Nucleus Basalis of Meynert Revisited: Anatomy, History and Differential Involvement in Alzheimer's and Parkinson's Disease." *Acta Neuropathologica* 129 (4): 527–40. https://doi.org/10.1007/s00401-015-1392-5.

Lyu, Wenjiao, Ye Wu, Khoi Minh Huynh, Sahar Ahmad, and Pew-Thian Yap. 2024. "A Multimodal Submillimeter MRI Atlas of the Human Cerebellum." *Scientific Reports* 14 (1): 5622. https://doi.org/10.1038/s41598-024-55412-y.

Markello, Ross D., Golia Shafiei, Christina Tremblay, Ronald B. Postuma, Alain Dagher, and Bratislav Misic. 2021. "Multimodal Phenotypic Axes of Parkinson's Disease." *Npj Parkinson's Disease* 7 (1): 1–12. https://doi.org/10.1038/s41531-020-00144-9.

Menke, Ricarda A., Jan Scholz, Karla L. Miller, Sean Deoni, Saad Jbabdi, Paul M. Matthews, and Mojtaba Zarei. 2009. "MRI Characteristics of the Substantia Nigra in Parkinson's Disease: A Combined Quantitative T1 and DTI Study." *NeuroImage* 47 (2): 435–41. https://doi.org/10.1016/j.neuroimage.2009.05.017.

Menze, Bjoern H., Andras Jakab, Stefan Bauer, Jayashree Kalpathy-Cramer, Keyvan Farahani, Justin Kirby, Yuliya Burren, et al. 2015. "The Multimodal Brain Tumor Image Segmentation Benchmark (BRATS)." *IEEE Transactions on Medical Imaging* 34 (10): 1993–2024. https://doi.org/10.1109/TMI.2014.2377694.

Mori, Susumu, Kenichi Oishi, and Andreia V. Faria. 2009. "White Matter Atlases Based on Diffusion Tensor Imaging." *Current Opinion in Neurology* 22 (4): 362–69. https://doi.org/10.1097/WCO.0b013e32832d954b.

Murphy, Keelin, Bram van Ginneken, Joseph M. Reinhardt, Sven Kabus, Kai Ding, Xiang Deng, Kunlin Cao, et al. 2011. "Evaluation of Registration Methods on Thoracic CT: The EMPIRE10 Challenge." *IEEE Transactions on Medical Imaging* 30 (11): 1901–20. https://doi.org/10.1109/TMI.2011.2158349.

Nemmi, F., A. Pavy-Le Traon, O. R. Phillips, M. Galitzky, W. G. Meissner, O. Rascol, and P. Péran. 2019. "A Totally Data-Driven Whole-Brain Multimodal Pipeline for the Discrimination of Parkinson's Disease, Multiple System Atrophy and Healthy Control." *NeuroImage: Clinical* 23 (January): 101858. https://doi.org/10.1016/j.nicl.2019.101858.

Noble, Stephanie, Dustin Scheinost, and R. Todd Constable. 2019. "A Decade of Test-Retest Reliability of Functional Connectivity: A Systematic Review and Meta-Analysis." *NeuroImage* 203 (December): 116157. https://doi.org/10.1016/j.neuroimage.2019.116157.

on behalf of the Parkinson's Progression Markers Initiative, Michael C. Brumm, Andrew Siderowf, Tanya Simuni, Elliot Burghardt, Seung Ho Choi, Chelsea Caspell-Garcia, et al. 2023. "Parkinson's Progression Markers Initiative: A Milestone-Based Strategy to Monitor Parkinson's Disease Progression." *Journal of Parkinson's Disease* 13 (6): 899–916. https://doi.org/10.3233/JPD-223433.

Owens-Walton, Conor, Talia M. Nir, Sarah Al-Bachari, Sonia Ambrogi, Tim J. Anderson, Ítalo Karmann Aventurato, Fernando Cendes, et al. 2024. "A Worldwide Study of White Matter Microstructural Alterations in People Living with Parkinson's Disease." medRxiv. https://doi.org/10.1101/2024.01.16.24301235.

Parkes, Linden, Ben Fulcher, Murat Yücel, and Alex Fornito. 2018. "An Evaluation of the Efficacy, Reliability, and Sensitivity of Motion Correction Strategies for Resting-State Functional MRI." *NeuroImage* 171 (May): 415–36. https://doi.org/10.1016/j.neuroimage.2017.12.073.

Pauli, Wolfgang M., Amanda N. Nili, and J. Michael Tyszka. 2018. "A High-Resolution Probabilistic in Vivo Atlas of Human Subcortical Brain Nuclei." *Scientific Data* 5 (1): 180063. https://doi.org/10.1038/sdata.2018.63.

Péran, Patrice, Andrea Cherubini, Francesca Assogna, Fabrizio Piras, Carlo Quattrocchi, Antonella Peppe, Pierre Celsis, et al. 2010. "Magnetic Resonance Imaging Markers of Parkinson's Disease Nigrostriatal Signature." *Brain* 133 (11): 3423–33. https://doi.org/10.1093/brain/awq212.

Pietracupa, Sara, Antonio Suppa, Neeraj Upadhyay, Costanza Giannì, Giovanni Grillea, Giorgio Leodori, Nicola Modugno, et al. 2018. "Freezing of Gait in Parkinson's Disease: Gray and White Matter Abnormalities." *Journal of Neurology* 265 (1): 52–62. https://doi.org/10.1007/s00415-017-8654-1.

Poston, Kathleen L., Matthew A. I. Ua Cruadhlaoich, Laura F. Santoso, Jeffrey D. Bernstein, Tian Liu, Yi Wang, Brian Rutt, Geoffrey A. Kerchner, and Michael M. Zeineh. 2020. "Substantia Nigra Volume Dissociates Bradykinesia

and Rigidity from Tremor in Parkinson's Disease: A 7 Tesla Imaging Study." *Journal of Parkinson's Disease* 10 (2): 591–604. https://doi.org/10.3233/JPD-191890.

Risacher, Shannon L., Wesley H. Anderson, Arnaud Charil, Peter F. Castelluccio, Sergey Shcherbinin, Andrew J. Saykin, and Adam J. Schwarz. 2017. "Alzheimer disease brain atrophy subtypes are associated with cognition and rate of decline." *Neurology* 89 (21): 2176–86. https://doi.org/10.1212/WNL.0000000000004670.

Rizvi, Batool, Mithra Sathishkumar, Soyun Kim, Freddie Márquez, Steven J. Granger, Myra S. Larson, Blake A. Miranda, et al. 2023. "Posterior White Matter Hyperintensities Are Associated with Reduced Medial Temporal Lobe Subregional Integrity and Long-Term Memory in Older Adults." *NeuroImage. Clinical* 37: 103308. https://doi.org/10.1016/j.nicl.2022.103308.

Ryman, Sephira G., and Kathleen L. Poston. 2020. "MRI Biomarkers of Motor and Non-Motor Symptoms in Parkinson's Disease." *Parkinsonism & Related Disorders* 73 (April): 85–93. https://doi.org/10.1016/j.parkreldis.2019.10.002.

Schwarz, Stefan T., Timothy Rittman, Vamsi Gontu, Paul S. Morgan, Nin Bajaj, and Dorothee P. Auer. 2011. "T1-Weighted MRI Shows Stage-Dependent Substantia Nigra Signal Loss in Parkinson's Disease." *Movement Disorders* 26 (9): 1633–38. https://doi.org/10.1002/mds.23722.

Shahnawaz, Mohammad, Abhisek Mukherjee, Sandra Pritzkow, Nicolas Mendez, Prakruti Rabadia, Xiangan Liu, Bo Hu, et al. 2020. "Discriminating α-Synuclein Strains in Parkinson's Disease and Multiple System Atrophy." *Nature* 578 (7794): 273–77. https://doi.org/10.1038/s41586-020-1984-7.

Shirer, William R., Heidi Jiang, Collin M. Price, Bernard Ng, and Michael D. Greicius. 2015. "Optimization of Rs-fMRI Pre-Processing for Enhanced Signal-Noise Separation, Test-Retest Reliability, and Group Discrimination." *NeuroImage* 117 (August): 67–79. https://doi.org/10.1016/j.neuroimage.2015.05.015.

Siderowf, Andrew, Luis Concha-Marambio, David-Erick Lafontant, Carly M. Farris, Yihua Ma, Paula A. Urenia, Hieu Nguyen, et al. 2023. "Assessment of Heterogeneity Among Participants in the Parkinson's Progression Markers Initiative Cohort Using α-Synuclein Seed Amplification: A Cross-Sectional Study." *The Lancet. Neurology* 22 (5): 407–17. https://doi.org/10.1016/S1474-4422(23)00109-6.

Simuni, Tanya, Lana M. Chahine, Kathleen Poston, Michael Brumm, Teresa Buracchio, Michelle Campbell, Sohini Chowdhury, et al. 2024. "A Biological Definition of Neuronal α-Synuclein Disease: Towards an Integrated Staging System for Research." *The Lancet Neurology* 23 (2): 178–90. https://doi.org/10.1016/S1474-4422(23)00405-2.

Sokołowski, Andrzej, Nikhil Bhagwat, Yohan Chatelain, Mathieu Dugré, Alexandru Hanganu, Oury Monchi, Brent McPherson, et al. 2024. "Longitudinal Brain Structure Changes in Parkinson's Disease: A Replication Study." *PLOS ONE* 19 (1): e0295069. https://doi.org/10.1371/journal.pone.0295069.

Stone, James R., Brian B. Avants, Nicholas J. Tustison, Jessica Gill, Elisabeth

A. Wilde, Kiel D. Neumann, Leslie A. Gladney, et al. 2023. "Neurological Effects of Repeated Blast Exposure in Special Operations Personnel." *Journal of Neurotrauma*, November. https://doi.org/10.1089/neu.2023.0309.

Stone, James R., Brian B. Avants, Nicholas J. Tustison, Eric M. Wassermann, Jessica Gill, Elena Polejaeva, Kristine C. Dell, et al. 2020. "Functional and Structural Neuroimaging Correlates of Repetitive Low-Level Blast Exposure in Career Breachers." *Journal of Neurotrauma* 37 (23): 2468–81. https://doi.org/10.1089/neu.2020.7141.

Tahmasian, Masoud, Lisa M. Bettray, Thilo van Eimeren, Alexander Drzezga, Lars Timmermann, Claudia R. Eickhoff, Simon B. Eickhoff, and Carsten Eggers. 2015. "A Systematic Review on the Applications of Resting-State fMRI in Parkinson's Disease: Does Dopamine Replacement Therapy Play a Role?" *Cortex* 73 (December): 80–105. https://doi.org/10.1016/j.cortex.2015.08.005.

Tanaka, Saori C., Ayumu Yamashita, Noriaki Yahata, Takashi Itahashi, Giuseppe Lisi, Takashi Yamada, Naho Ichikawa, et al. 2021. "A Multi-Site, Multi-Disorder Resting-State Magnetic Resonance Image Database." *Scientific Data* 8 (1): 227. https://doi.org/10.1038/s41597-021-01004-8.

Tolosa, Eduardo, Miquel Vila, Christine Klein, and Olivier Rascol. 2020. "LRRK2 in Parkinson Disease: Challenges of Clinical Trials." *Nature Reviews Neurology* 16 (2): 97–107. https://doi.org/10.1038/s41582-019-0301-2.

Tong, Qiqi, Hongjian He, Ting Gong, Chen Li, Peipeng Liang, Tianyi Qian, Yi Sun, Qiuping Ding, Kuncheng Li, and Jianhui Zhong. 2019. "Reproducibility of Multi-Shell Diffusion Tractography on Traveling Subjects: A Multicenter Study Prospective." *Magnetic Resonance Imaging* 59 (June): 1–9. https://doi.org/10.1016/j.mri.2019.02.011.

Tremblay, Christina, Nooshin Abbasi, Yashar Zeighami, Yvonne Yau, Mahsa Dadar, Shady Rahayel, and Alain Dagher. 2020. "Sex Effects on Brain Structure in de Novo Parkinson's Disease: A Multimodal Neuroimaging Study." *Brain* 143 (10): 3052–66. https://doi.org/10.1093/brain/awaa234.

Tustison, Nicholas J., Philip A. Cook, Andrew J. Holbrook, Hans J. Johnson, John Muschelli, Gabriel A. Devenyi, Jeffrey T. Duda, et al. 2021. "The ANTsX Ecosystem for Quantitative Biological and Medical Imaging." *Scientific Reports* 11 (1). https://doi.org/10.1038/s41598-021-87564-6.

Tustison, Nicholas J., Michael A. Yassa, Batool Rizvi, Philip A. Cook, Andrew J. Holbrook, Mithra T. Sathishkumar, Mia G. Tustison, James C. Gee, James R. Stone, and Brian B. Avants. 2023. "ANTsX Neuroimaging-Derived Structural Phenotypes of UK Biobank." medRxiv. https://doi.org/10.1101/2023.01.17.23284693.

Veitch, Dallas P, Michael W Weiner, Melanie Miller, Paul S Aisen, Miriam A Ashford, Laurel A Beckett, Robert C Green, et al. 2024. "The Alzheimer's Disease Neuroimaging Initiative in the Era of Alzheimer's Disease Treatment: A Review of ADNI Studies from 2021 to 2022." *Alzheimer's & Dementia* 20 (1): 652–94.

Wang, Shuaiwen, Yanli Zhang, Junqiang Lei, and Shunlin Guo. 2021. "Investigation of Sensorimotor Dysfunction in Parkinson Disease by Resting-State

fMRI." *Neuroscience Letters* 742 (January): 135512. https://doi.org/10.1016/j.neulet.2020.135512.

Xie, Yihui, Christophe Dervieux, and Emily Riederer. 2020. *R Markdown Cookbook*. Boca Raton, Florida: Chapman; Hall/CRC. https://bookdown.org/yihui/rmarkdown-cookbook.

Yan, Xiaoxuan, Ru Kong, Aihuiping Xue, Qing Yang, Csaba Orban, Lijun An, Avram J. Holmes, et al. 2023. "Homotopic Local-Global Parcellation of the Human Cerebral Cortex from Resting-State Functional Connectivity." *NeuroImage* 273 (June): 120010. https://doi.org/10.1016/j.neuroimage.2023.120010.

Zaborszky, Laszlo, L. Hoemke, H. Mohlberg, A. Schleicher, K. Amunts, and K. Zilles. 2008. "Stereotaxic Probabilistic Maps of the Magnocellular Cell Groups in Human Basal Forebrain." *NeuroImage* 42 (3): 1127–41. https://doi.org/10.1016/j.neuroimage.2008.05.055.